Progress in Oceanography 138 (2015) 176–193

Contents lists available at ScienceDirect

Progress in Oceanography

journal homepage: www.elsevier.com/locate/pocean

Model investigations of the North Atlantic spring bloom initiation

Angela M. Kuhn *, Katja Fennel, Jann Paul Mattern [1]

Department of Oceanography, Dalhousie University, PO Box 15000, Halifax, NS B3H 4R2, Canada

ARTICLE INFO

Article history:
Received 9 December 2014
Received in revised form 14 July 2015
Accepted 14 July 2015
Available online 21 July 2015

ABSTRACT

The spring bloom – a massive growth of phytoplankton that occurs annually during the spring season in mid and high latitudes – plays an important role in carbon export to the deep ocean. The onset of this event has been explained from bottom-up and top-down perspectives, exemplified by the "critical-depth" and the "dilution-recoupling" hypotheses, respectively. Both approaches differ in their key expectations about how seasonal fluctuations of the mixed layer affect the plankton community. Here we assess whether the assumptions inherent to these hypotheses are met inside a typical onedimensional Nutrient–Phytoplankton–Zooplankton–Detritus (NPZD) model, optimized to best represent climatological annual cycles of satellite-based phytoplankton biomass in the Subpolar North Atlantic. The optimized model is used in idealized experiments that isolate the effects of mixed layer fluctuations and zooplankton grazing, in order to elucidate their significance. We analyzed the model sensitivity qualitatively and using a second-order Taylor series decomposition of the model equations. Our results show that the conceptual bases of both bottom-up and top-down approaches are required to explain the process of blooming; however, neither of their bloom initiation mechanisms fully applies in the experiments. We find that a spring bloom can develop in the absence of mixed layer fluctuations, and both its magnitude and timing seem to strongly depend on nutrient and light availability. Furthermore, although zooplankton populations modulate the phytoplankton concentrations throughout the year, directly prescribed and physically driven changes in zooplankton grazing do not produce significant time shifts in bloom initiation, as hypothesized. While recognizing its limitations, our study emphasizes the processes that require further testing in order to discern among competing hypotheses.

1. Introduction

The annually occurring massive growth of phytoplankton during spring in mid and high latitudes, referred to as the spring bloom, is recognized as key to better understand the uncertainties concerning the oceanic carbon cycle and its consequent climate feedbacks under global warming scenarios (Joos et al., 1999; Maier-Reimer et al., 1996; Sarmiento et al., 1998). However, the mechanisms that determine when and how the spring bloom initiates are not yet agreed upon. The traditional model for bloom initiation is based on the concept that there exists a critical depth at which vertically integrated phytoplankton production equals phytoplankton losses. According to this conceptual model, the spring bloom can occur only when the depth of the mixed layer is smaller than this critical depth, allowing phytoplankton production to exceed losses by spending enough time in the euphotic zone (Sverdrup, 1953). Under the assumptions of a constant ratio between phytoplankton growth and loss rates and a thoroughly mixed layer, Sverdrup estimated that this condition is not met during periods of deep mixing in winter, before thermal stratification establishes in spring.

The bottom-up control of bloom dynamics implied by Sverdrup's critical depth model has been a cornerstone of marine ecology for more than half a century. Nevertheless, it has been criticized for its inability to explain observations of phytoplankton growth before the onset of stable stratification (Garside and Garside, 1993; Townsend et al., 1992; Behrenfeld, 2010). Several studies diverge only nominally from the original critical depth model, suggesting that weak or temporary stratification can be sufficient to initiate blooms in winter (Colebrook, 1979; Townsend et al., 1992; Wasmund et al., 1998). Along that same line of thought, Huisman et al. (1999a,b, 2002) argued that there exists a critical turbulence level, below which phytoplankton growth can occur in winter. Attention has also been called to the difference between mixed layer and the mixing or turbulent layer (Brainerd and Gregg, 1995) suggesting that after the mixed layer reaches its maximum depth, the bloom can be triggered by a shutdown of turbulent convection (Fennel, 1999; Taylor and Ferrari, 2011a) or by mixing occurring only in surface layers (Chiswell, 2011).

* Corresponding author. Tel.: +1 902 4943655.
E-mail address: angela.kuhn@dal.ca (A.M. Kuhn).
[1] Present address: Ocean Sciences Department, University of California, Santa Cruz, CA, USA.

http://dx.doi.org/10.1016/j.pocean.2015.07.004
0079-6611/

Others have argued that strong winter convection actually enhances the chances of sinking phytoplankton to be transported back into the euphotic zone and receive light (Backhaus et al., 2003; Lande and Wood, 1987). The latter idea is consistent with theoretical and observational considerations about the annual succession of phytoplankton species, which postulate that non-motile diatoms benefit from turbulent, high-nutrient conditions while motile cells dominate during stratified, low-nutrient periods (Margalef, 1978; Ward and Waniek, 2007).

The discussion about the causes of spring bloom initiation was reinvigorated by analyses that departed from assuming a bottom-up system controlled by vertical mixing and light, as portrayed in the classical critical-depth model. Top-down control by zooplankton (e.g., Banse, 1994) regained interest with the formulation of the dilution-recoupling hypothesis (Behrenfeld, 2010; Boss and Behrenfeld, 2010; Mariani et al., 2013), which suggests that mixed layer deepening plays a dominant role in bloom initiation by forcing the dilution of phytoplankton and zooplankton during winter. As is known from incubation experiments (e.g., Landry and Hassett, 1982), such dilution negatively affects grazing success and may reduce phytoplankton losses enough for positive net phytoplankton growth to occur in the open ocean in winter (Behrenfeld, 2010). The dilution-recoupling hypothesis has since broadened, recognizing that the decoupling of planktonic feedbacks through dilution is one of many physical and ecological disturbances that continuously act together to determine the initiation, development rate and climax of blooms (Behrenfeld et al., 2013).

Our objective in the present study is to assess which of the assumptions inherent to the bottom-up and top-down theoretical approaches are met inside a typical numerical ecosystem model or, in other words, whether and under what conditions the different mechanisms of spring bloom initiation occur. The model's low computational cost and flexibility allows us to perform a set of idealized experiments designed to isolate the effects of mixed layer depth fluctuations and zooplankton grazing on bloom initiation. We use a vertically resolved Nutrient–Phytoplankton–Zooplankton–Detritus (NPZD) model, resembling those used in early studies on model behavior (Evans and Parslow, 1985; Franks et al., 1986; Steele and Henderson, 1992). NPZD models also form the base for functional-type ecosystem models (e.g., Fasham et al., 1990; Fennel et al., 2006) now widely used in coupled physical–biological climate models (Bopp et al., 2005; Doney et al., 1996; Franks et al., 2013). Even the simplest of these models rely on a number of parameters with values that are either poorly known or exhibit a large range in the experimental and field literature due to taxonomical differences, date and location of sampling or methodological constraints (e.g., Fahnenstiel et al., 1995; Putland, 2000; Sarthou et al., 2005). For that reason, model optimization techniques are increasingly used to objectively define model parameters (Bagniewski et al., 2011; Fennel et al., 2001; Friedrichs et al., 2007; Schartau et al., 2001; Ward et al., 2010). Here we follow this approach and apply an evolutionary algorithm for model optimization based on climatological values of observed surface chlorophyll in the Subpolar North Atlantic. We further investigate the sensitivity of the model using a second-order Taylor series decomposition to identify the variables that influence the simulated phytoplankton annual cycle most strongly.

Our results are in line with the view of the spring bloom as the climax of a continuous process in which bottom-up and top-down forcings act simultaneously (Behrenfeld et al., 2013; Riley, 1965; Strom, 2002), and different processes dominate at different points in time to shape the annual cycle of phytoplankton biomass. The conceptual bases of both the critical-depth and the dilution-recoupling hypotheses are shown to be true within our modeling framework; however, neither of their bloom initiation mechanisms fully applies in the experiments.

The mechanisms through which a simple model like the one we examine here develops a spring bloom could differ from those at play in reality. Rather than providing a new explanation for the spring bloom initiation, this analysis is aimed at emphasizing the processes that require further testing in more realistic models and using observational data sets. The remainder of this manuscript is organized as follows: Section 2 describes the methods used in the study, including the configuration of the base model; Section 3 describes the optimized model results and their sensitivity to parameters and variables; in Section 4 we describe the idealized experiments' configuration and results. Discussion and final conclusions are presented in Sections 5 and 6.

2. Methods

2.1. Data sets

Our study region is the North Atlantic Ocean, between 40°N–50°N and 45°W–15°W (Fig. 1). We analyze models for six of the twelve 5° latitude by 10° longitude bins presented in Behrenfeld (2010), using satellite-based phytoplankton biomass observations and mixed layer depth climatologies from the same study. Our analysis includes the lower latitude bins (NA1–NA3) located at the transition zone from subtropical to subpolar bloom regimes (Henson et al., 2009); and the subpolar region characterized by higher chlorophyll in bins NA4–NA6. The bins north of 50°N are not used because chlorophyll observations in winter are missing.

The satellite-based phytoplankton biomass climatology (P^{obs}) is used to optimize the biological parameters of the base model described in Section 2.2, whereas the mixed layer depth climatology (H_{MLD}) is used as a model forcing variable to impose time- and depth-varying diffusivities. For details on these climatologies we refer the reader to Behrenfeld (2010) and http://www.science.oregonstate.edu/ocean.productivity/. In general, the P^{obs} climatology is based on eight-day Sea-viewing Wide Field-of-view (SeaWiFS) satellite chlorophyll values from January 1998 to December 2006, spatially averaged for each bin. From there, phytoplankton carbon concentrations were derived by Behrenfeld (2010) using the Garver–Siegel–Maritorena algorithm for particulate backscattering coefficients (Behrenfeld et al., 2005; Garver and Siegel, 1997; Maritorena et al., 2002). We transformed the phytoplankton carbon concentrations into nitrogen units (mmol N m^{-3}) using the Redfield ratio (106C:16N) and linearly interpolated the eight-day data to daily resolution for comparison with the model output. Although phytoplankton carbon biomass estimates derived from scattering properties may be influenced by the particle size distribution (Dall'Olmo et al., 2009), they have been shown to represent phytoplankton biomass well (Behrenfeld and Boss, 2006, 2003; Siegel et al., 2005; Westberry et al., 2008). Comparing the model results against such estimates, instead of satellite chlorophyll, also avoids further model assumptions about the C:Chl ratio, as chlorophyll concentrations may vary independently from biomass due to physiological changes driven by light and nutrient availability (Geider, 1987; Geider et al., 1997; Wang et al., 2009).

We also use the corresponding mixed layer depth climatology for each bin, which was constructed using output from the Simple Ocean Data Assimilation (SODA) model (1998–2004) and the Fleet Numerical Meteorology and Oceanography Center (FNMOC) model (2005–2006) (see Behrenfeld, 2010 and citations therein). Both models are data-assimilative (i.e., they incorporate available observations to attain the best possible representation of the ocean state), and the resulting mixed layer depth climatology agrees well with climatological values derived from available high vertical resolution temperature and salinity profiles from 1941 to 2002 (de Boyer Montégut et al., 2004). In addition, sea temperature profiles

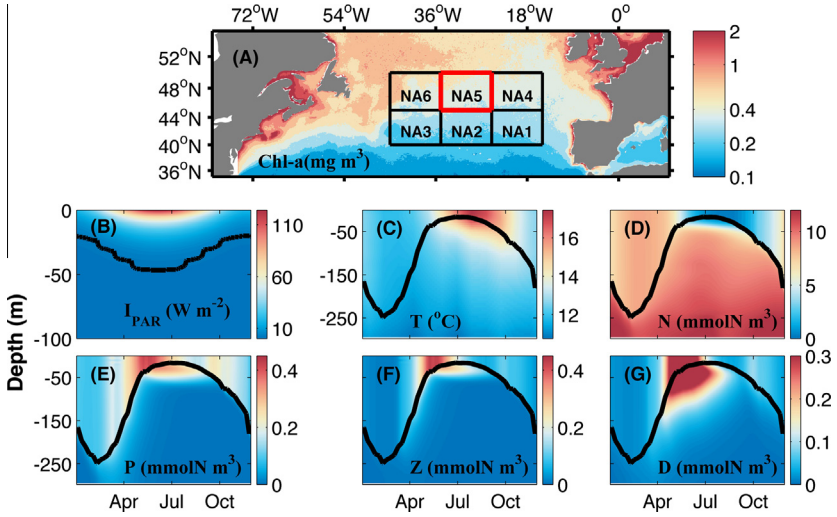

Fig. 1. (A) Location of the study bins showing, as a reference, the mean annual surface chlorophyll concentration (Chl-a, mg m^{-3}) calculated from eight-day resolution SeaWiFS satellite data from January 1998 to December 2006. The northern bins exhibit higher mean annual chlorophyll than the southern bins. Subplots (B)–(G) correspond to bin NA5. (B) Simulated average daily photosynthetic active radiation (I_{PAR}, W m^{-2}). This subplot is restricted to the top 100 m of the water column, and shows the depth of the euphotic zone defined as the depth at which light limitation is lower than 1% ($Lim_I \leqslant 10^{-2}$, solid line). (C) Climatological WOA temperature (T, °C). Optimized NPZD model daily averaged concentrations of (D) nutrients, (E) phytoplankton, (F) zooplankton, and (G) detritus in mmol N m^{-3}. The black solid lines in panels (C)–(G) show the climatological mixed layer depth.

from the World Ocean Atlas 2009 (WOA) climatology provide physical forcing to our model, and WOA nitrate profiles (Garcia et al., 2010) are used to restore nutrient concentrations at depth.

2.2. Base model description

We use a vertically resolved NPZD model to replicate the climatological annual cycles of satellite-based phytoplankton biomass in our study bins. While more complex models (i.e., those that simulate more state variables and pathways) may be more realistic than this simple NPZD model, the increased complexity adds more parameterizations and more poorly known parameters (Denman, 2003; Anderson, 2005). Choosing a simple model makes it easier to constrain the model dynamics with limited observations, and allows for easier exploration and interpretation of the effects of perturbing isolated variables.

The model simulates the top 300 m of the ocean with a vertical resolution of 5 m. The vertical grid is divided into two distinct layers: a turbulent surface mixed layer (layer 1) and a quiescent layer below (layer 2). The annual cycle of mixed layer depth (H_{MLD}) is imposed and determines how many grid cells are in each layer at a given point in time. A high diffusivity is assigned to all grid cells above the prescribed H_{MLD} (representing the active layer 1) and ensures complete mixing within the mixed layer on a time scale of 1 day ($k_{D1} = H_{MLD}{}^2\ \mathrm{d}^{-1}$). A low diffusivity ($k_{D2} = k_{D1} \times 10^{-3}$) is assigned to all grid cells below (representing the quiescent layer 2). All biological parameters and other symbols used throughout the text are listed in Table 1.

Phytoplankton and zooplankton prey–predator dynamics are represented as follows:

$$\frac{\partial P}{\partial t} = \mu_{max} Lim_N Lim_I P - gZ - l_{PN}P - l_{PD}P - w_P \frac{\partial P}{\partial z} + \frac{\partial}{\partial z}\left(k_D \frac{\partial P}{\partial z}\right) \quad (1)$$

$$\frac{\partial Z}{\partial t} = \beta g Z - l_{ZN}Z - l_{ZD}Z^2 + \frac{\partial}{\partial z}\left(k_D \frac{\partial Z}{\partial z}\right) \quad (2)$$

where the phytoplankton maximum growth rate (μ_{max}) is modulated by nutrient limitation (Lim_N) and light limitation (Lim_I) factors. Nutrient limitation follows $Lim_N = \frac{N}{k_N + N}$, where k_N is the half-saturation constant for nutrient uptake. Light limitation is formulated as $Lim_I = \frac{\alpha I_{PAR}}{\sqrt{\mu_{max}^2 + \alpha^2 I_{PAR}^2}}$ (Evans and Parslow, 1985; Smith, 1936), where the photosynthetically active radiation (I_{PAR}) is a fraction equal to 43% of the total solar radiation. PAR decreases exponentially with depth (z) according to $PAR(z) = 0.43 I_0^{-zk_I}$, where $k_I = 0.1\ \mathrm{m}^{-1}$ is the light attenuation coefficient. I_0 is the total incoming solar radiation below the sea surface; it is simulated using the astronomical formula (Brock, 1981), allowing for diel variations and assuming a 40% attenuation by the atmosphere and a solar constant of 1366.1 W m^{-2}. Temperature dependency of the maximum growth rate of phytoplankton is included by a Q_{10} formulation according to $\mu_{max} = \mu_0\ 1.88^{T/10\ ^\circ\mathrm{C}}$ (Eppley, 1972), where μ_0 is the maximum growth rate at 0 °C. The parameters l_{PN}, l_{PD} are the metabolic loss and mortality rates of phytoplankton, and depend on temperature according to the same Q_{10} formulation as μ_{max}. Phytoplankton metabolic losses feed into the nutrient pool, while mortality losses feed into the detritus pool. The last two terms of Eq. (1) represent phytoplankton sinking at a speed w_P and vertical mixing.

In Eq. (2), zooplankton grazing follows a sigmoidal functional form $g = g_{max} \frac{P^2}{k_P^2 + P^2}$, where g_{max} is the maximum grazing rate and k_P is the half-saturation for phytoplankton ingestion. Zooplankton assimilates only a fraction β of the total consumed phytoplankton; the rest enters the detritus pool. The parameters l_{ZN} and l_{ZD} represent zooplankton excretion and mortality rates, which feed into the nutrient and detritus pools, respectively. They also depend on temperature according to the Q_{10} formulation described above. The equations for detritus and nutrients are:

$$\frac{\partial D}{\partial t} = ((1-\beta)g + l_{ZD}Z)Z + l_{PD}P - r_{DN}D - w_D \frac{\partial D}{\partial z} + \frac{\partial}{\partial z}\left(k_D \frac{\partial D}{\partial z}\right) \quad (3)$$

$$\frac{\partial N}{\partial t} = -\mu_{max} Lim_N Lim_I P + l_{PN}P + l_{ZN}Z + r_{DN}D + \frac{\partial}{\partial z}\left(k_D \frac{\partial N}{\partial z}\right) + \gamma(N_{WOA} - N) \quad (4)$$

Table 1
Ecosystem model parameters and symbols used throughout the text. For parameters that were optimized the allowed range during the optimization is shown.

Parameter	Description	Range or value	Units
Phytoplankton (P) parameters			
α	Initial photosynthetic slope	0.02–0.25[a,b]	$(W\ m^{-2})^{-1}\ d^{-1}$
μ_0	Maximum growth rate at $T = 0$ °C	0.02–2.0[c,d,e]	d^{-1}
k_N	Half-saturation coefficient of nutrient uptake	0.05–3.5[c]	$mmol\ N\ m^{-3}$
l_{PN}	Phytoplankton respiration rate at $T = 0$ °C	0.005–0.25[c]	d^{-1}
l_{PD}	Phytoplankton mortality rate at $T = 0$ °C	0.01–0.25[f]	d^{-1}
w_P	Sinking rate of phytoplankton	0.025–2.5[c,g,h,i,j]	$m\ d^{-1}$
Zooplankton (Z) parameters			
g_{max}	Maximum grazing rate	0.2–3.0[c,d,k,l]	d^{-1}
k_P	Half-saturation coefficient of grazing	0.5–5.0[a]	$mmol\ N\ m^{-3}$
β	Zooplankton assimilation efficiency	0.25–0.95[m,n]	Non-dimensional
l_{ZN}	Zooplankton excretion rate at $T = 0$ °C	0.01–0.25[a]	d^{-1}
l_{ZD}	Zooplankton mortality rate at $T = 0$ °C	0.02–0.35[a,b]	d^{-1}
Detritus (D) parameters			
r_{DN}	Remineralization rate	0.015–0.15[b]	d^{-1}
w_D	Sinking rate of detritus	0.05–25[a]	$m\ d^{-1}$
Additional symbols and non-optimized parameters			
P^{obs}	Phytoplankton biomass climatology from satellite	–	$mmol\ N\ m^{-3}$
T	WOA temperature climatology	–	°C
N_{WOA}	WOA NO_3 climatology	–	$mmol\ N\ m^{-3}$
H_{MLD}	SODA and FNMOC mixed layer depth climatology	–	m
I_0	Total incoming solar radiation at the ocean's surface	–	$W\ m^{-2}$
I_{PAR}	Photosynthetic active radiation	–	$W\ m^{-2}$
Lim_I	Light limitation factor for phytoplankton growth	–	Non-dimensional
Lim_N	Nutrient limitation factor for phytoplankton growth	–	Non-dimensional
k_{D1}	Diffusivity coefficient above the mixed layer depth	–	$m^2\ d^{-1}$
k_{D2}	Diffusivity coefficient below the mixed layer depth	–	$m^2\ d^{-1}$
k_I	Light attenuation coefficient	0.1[o]	m^{-1}
γ	Nudging strength	Eq. (5)	d^{-1}
R	Vertically integrated phytoplankton growth minus vertically integrated phytoplankton losses	Eq. (9)	$mmol\ N\ m^{-2}$
H_{cr}	Critical-depth, defined as the depth at which $R = 0$	–	m
H_{euph}	Depth of the euphotic zone, defined as the depth at which $Lim_I < 1\%$	–	m
Optimization			
p	Parameter set (P, Z, and D parameters in this table)	–	–
$F(p)$	Cost value of parameter set p	Eq. (6)	–
P^{sim}	Simulated surface phytoplankton in the cost function	–	$mmol\ N\ m^{-3}$
w	Weight in the cost function	–	$(m^3\ (mmol\ N)^{-1})^2$
$NA\#_p$	Individually optimized parameter set	–	–
$\sum NA_p$	Jointly optimized parameter set	–	–
Sensitivity analyses			
$\Delta max(P)$	Change in maximum annual surface phytoplankton concentrations	–	$mmol\ N\ m^{-3}$
$\Delta max(r^*)$	Change in maximum annual phytoplankton inventory accumulation rates	–	d^{-1}
ΔDay^{P*}	Change in the date of bloom initiation according to Day^{P*}	–	Year day
ΔDay^{r*}	Change in the date of bloom initiation according to Day^{r*}	–	Year day
φ	System state in the Taylor decomposition analysis	–	–
$\vec{x}$	Vector of the model's variables in the Taylor decomposition analysis	–	–
Bloom timing metrics			
Normalized P	Normalized annual cycle of surface phytoplankton biomass used to define Day^{P*}	Eq. (7)	Non-dimensional
r^*	Phytoplankton inventory accumulation rate[p], shortly referred as accumulation rate, used to define Day^{r*}	–	d^{-1}
Day^{P*}	Date of bloom initiation, biomass-based metric	–	Julian days
Day^{r*}	Date of bloom initiation, phytoplankton inventory accumulation rate metric	–	Julian days
Experimental simulations			
ξ	Zooplankton accumulation term or entrainment	Exp. I	$mmol\ N\ m^{-3}\ d^{-1}$
$\frac{\xi}{Z\beta g}$	Zooplankton entrainment over grazing	Exp. I	Non-dimensional
Z_{total}	Total zooplankton biomass in the mixed layer	Exp. III	$mmol\ N\ m^{-2}$
H^*_{MLD}	Idealized mixed layer depth	Exp. III	m

Sources:
[a] Fennel et al. (2006).
[b] Schartau and Oschlies (2003).
[c] Sarthou et al. (2005).
[d] Fahnenstiel et al. (1995).
[e] Veldhuis et al. (2005).
[f] Bagniewski et al. (2011).
[g] Smayda (1974).
[h] Bienfang (1981).
[i] Smayda and Bienfang (1983).
[j] Walsby and Holland (2006).
[k] Gifford et al. (1995).
[l] Nejstgaard et al. (2001, 1997).
[m] Landry et al. (1984).
[n] Tande and Slagstad (1985).
[o] Evans and Parslow (1985).
[p] Behrenfeld (2010).

Sources of the detrital pool are phytoplankton mortality ($l_{PD}\ P$), zooplankton mortality ($l_{ZD}\ Z^2$) and the fraction of unassimilated ingestion ($(1-\beta)\ g\ Z$), which represents sloppy feeding and egested fecal pellets. Detritus is remineralized back to the nutrient pool at the rate r_{DN} and sinks at a velocity of w_D (Eq. (3)). Taking into account the limitations of our one-dimensional model, simulated subsurface nutrient concentrations are weakly nudged to the WOA nitrate climatology with the term $\gamma(N_{WOA}-N)$ in Eq. (4). The highest nudging strength is applied to the bottom grid cells, lower nudging strength to the mid-water grid cells and no nudging to the surface according to:

$$\gamma = \begin{cases} 0, & for\ z < \min(H_{MLD}) \\ \frac{1}{90d}, & for\ \min(H_{MLD}) \leqslant z < \max(H_{MLD}) \\ \frac{1}{30d}, & for\ z \leqslant \max(H_{MLD}) \end{cases} \quad (5)$$

where $\min(H_{MLD})$ and $\max(H_{MLD})$ are the minimum and maximum depth of the mixed layer during the annual cycle.

2.3. Optimization method

The model is optimized for each of the 6 bins shown in Fig. 1A, such that the simulated annual cycles of surface phytoplankton best reproduce the available observations. In general, a parameter optimization consists of systematically adjusting the model parameters, in order to minimize a cost function that measures the mismatch between observations and their model counterparts. The model spins up for 7 years to reach dynamical steady state and, once it has reached equilibrium, an additional year of model output is used to calculate the cost function ($F(p)$), which is defined as:

$$F(p) = \sum_{i=1}^{n} w_i \left(P_i^{obs} - P_i^{sim}(p)\right)^2 \quad (6)$$

where p is a vector that contains the 13 unknown biological parameters described in Table 1; $n = 365$ is the number of days in the annual cycle; P^{obs} is Behrenfeld (2010)'s satellite-based phytoplankton carbon biomass climatology transformed into units of nitrogen; and P^{sim} are our daily averages of the surface phytoplankton concentrations simulated using each p. To emphasize the initiation of the spring bloom, we assign a higher weight $w_i = 3$ $(m^3(mmol\ N)^{-1})^2$, $i = 1,\ldots,150$ to the first 150 days, while $w_i = 1$ $(m^3(mmol\ N)^{-1})^2$, $i = 151,\ldots,365$ is used for the rest of the year.

The optimization is implemented using an evolutionary algorithm, which borrows large part of its terminology from ecological sciences. In this section only, these terms are used in the context of the optimization method. The evolutionary algorithm simulates a process of natural selection by imposing a "survival of the fittest" strategy (Houck et al., 1995) on a population composed of different parameter sets p. Each p represents an individual within the population, here including a total of 30 parameter sets. The initial parameter population is randomly generated within a range of minimum and maximum parameter values that we chose based on observational and modeling literature (Table 1). Every iteration of the algorithm represents a generation of the parameter population, where the top 15 parameter sets with the smallest cost function values are allowed to survive and become parents of the next generation. Parent parameter sets reproduce and create an offspring by a crossover mechanism: each parameter in a new offspring parameter set is randomly drawn from either one of two randomly chosen parents. Offspring is produced until the population is replenished to its full size. Additionally, the offspring parameter sets are subjected to random mutations in 6 of their 13 parameter values by adding normally distributed random values with zero mean and a standard deviation of 5% of the respective parameter's range.

As the model is compared only to phytoplankton surface observations, it is difficult to effectively constrain the complete set of parameters. Ward et al. (2010) concluded that there is not a perfect solution to deal with the problem of under-determination of model parameters: if only a subset of parameters is optimized and the unconstrained parameters are fixed to precise values, the model cost is strongly affected by these default values. As parameters may co-vary during their evolution (e.g., Schartau and Oschlies, 2003), fixing some parameters will also affect the optimized parameter values. For these reasons, specifying the possible range of parameter values becomes important (Fennel et al., 2001; Schartau et al., 2001; Schartau and Oschlies, 2003). Within our algorithm, the minimum and maximum range is enforced after the mutation step to avoid unrealistic parameter values; when a parameter value is outside of its range, it is replaced by the corresponding minimum or maximum limit, plus or minus a uniformly distributed random value multiplied by 1% of the parameter range. In comparison to gradient descent methods, the algorithm allows a free random exploration of the whole parameter space defined by the possible range of parameter values, and is less prone to finding local optima (Ward et al., 2010).

We individually ran three replicate optimizations of 200 generations of the algorithm for each spatial bin (parameter sets $NA1_p$–$NA6_p$). An additional optimization was performed jointly for all bins ($\sum NA$), using a joint cost function that is the sum of the individual cost functions $F(p)$ for each bin. In all cases, the algorithm rapidly minimizes differences between the observations and model output within approximately 10 generations and the variance in the cost values of the parent population decreases significantly after 20 generations. For example, in bin NA5 the variance in the cost values of the parent population decreases from $\sigma^2 = 85.91$ $(mmol\ N\ m^{-3})^2$ to $\sigma^2 = 0.06$ $(mmol\ N\ m^{-3})^2$ after 20 generations. At the end of the algorithm, the individual optimizations show an average cost reduction of 87.8 ± 10%, while the joint optimization reduces the cost function by 86%.

2.4. Base model sensitivity

We estimate the sensitivity of the model results to the biological parameters qualitatively by doubling and halving each optimal parameter value and rerunning the model (Section 3.2). We also analyzed the model sensitivity to perturbations in forcing and state variables using a second-order Taylor series expansions of the system of equations (Section 3.3).

Taylor series expansions have been used to evaluate non-linear radiative feedbacks in atmospheric models (Colman et al., 1997) and interannual variability in air–sea CO_2 flux in a biogeochemical ocean model (Previdi et al., 2009). For this analysis, we denote our non-linear model as $\frac{\partial \vec{x}}{\partial t} = \varphi(\vec{x})$ where $\vec{x}$ is the vector of state variables including N, P, Z, D, PAR, T and H_{MLD}. A small perturbation of the model state, $\delta\vec{x}$, will produce a change $\delta\varphi$ in the model dynamics, that can be approximated by the first two terms of the Taylor Series:

$$\delta\varphi(\vec{x}) \approx \sum_{i=1}^{n} \frac{\partial\varphi(\vec{x})}{\partial x_i}\delta x_i + \frac{1}{2}\sum_{i=1}^{n}\sum_{j=1}^{n} \frac{\partial^2\varphi(\vec{x})}{\partial x_i \partial x_j}\delta x_i \delta x_j \quad (7)$$

The first-order partial derivatives provide estimates of the model's sensitivity to a change in each individual variable; the second-order derivatives provide an indication of how the model's sensitivity to changes in x_i depends on x_j and vice versa. We perturb each variable individually by +10% of its annual range (for H_{MLD}) or its range at the surface (for the vertically resolved variables). The perturbations are imposed over the optimized steady cycle solution throughout the whole year and at all depths (for the vertically resolved variables).

2.5. Spring bloom initiation metrics

In our analysis of spring bloom initiation we use two timing metrics, which have been previously used in the literature: (1) the day when a surface phytoplankton concentration threshold is exceeded (Day^{P*}) and (2) the day when the net phytoplankton accumulation rate becomes positive (Day^{r*}). Defining when the spring bloom effectively starts or which of these two metrics should be used to define it is not an objective of this study and left to other investigators (e.g., Brody et al., 2013). The metrics are intended to evaluate the effects of different processes on spring bloom initiation.

The concentration threshold is a commonly used metric defining bloom initiation as the first day that concentrations rise more than 5% above the median of the annual cycle (Henson et al., 2009, 2006; Platt et al., 2009; Siegel et al., 2002). A drawback of this method is that the amplitude and duration of the bloom affect the threshold value and thus can compromise the ability of this method to identify timing dissimilarities between individual annual cycles, as illustrated by Brody et al. (2013). While this is not a problem when comparing observations and optimized model results, which have similar threshold values, the experimental simulations discussed in Section 4 exhibit a large range of annual amplitudes and bloom characteristics. In order to use the same threshold metric for both optimized and experimental simulations, we define the bloom onset, Day^{P*}, after normalizing the simulated surface phytoplankton annual cycles according to:

$$normalized\ P = \frac{P - \min(P)}{\max(P) - \min(P)} \tag{8}$$

The threshold for bloom onset is then defined as 5% above the median of the normalized annual cycle.

The second metric of bloom timing, Day^{r*}, identifies the date when the transition from a decreasing to an increasing phytoplankton inventory occurs. It is based on the phytoplankton inventory accumulation rate (r^*), which is defined as the rate of change of vertically integrated phytoplankton. While this inventory value can be calculated from model output, satellite observations do not provide information of the phytoplankton vertical structure, thus we approximate r^* as in Behrenfeld (2010) and Behrenfeld et al. (2013). The time-varying depth of the euphotic zone required for this calculation is defined as the depth at which $Lim_I \leqslant 10^{-2}$ (see Fig. 1B). We smooth high frequency variability in r^* by applying a 90-day boxcar averaging, and Day^{r*} is then defined as the first day (in between one spring bloom and the next) when r^* becomes positive (Fig. 3).

2.6. Experimental simulations

Using the optimized models as a base, we proceed to perform three experiments aimed to examine whether and under what conditions the bloom initiation mechanisms portrayed in the critical-depth and dilution-recoupling hypotheses occur in the system. The experiments are summarized in Table 4, and changes made to the model configurations in order to run each experiment are explained along the experiments' results in Section 4. Experiment I tests the addition of a mechanism that concentrates zooplankton in response to a shoaling mixed layer. Experiment II evaluates the system's response in the absence of mixed layer fluctuations. The final Experiment III further focuses on the effects of direct and physically driven changes in zooplankton biomass, forcing them to be completely decoupled from changes in food availability. Results of the experiments are here exemplified using bin NA5 and are consistent over all bins (Appendix B).

3. Optimized simulation results

3.1. Plankton annual cycles

In general, the optimized simulations represent the observed surface phytoplankton well (Fig. 2), especially during the spring bloom initiation. The solutions also show low bias and root-mean-square errors, and are highly correlated with the observations (Table 2), accomplishing the purpose of the optimization algorithm. The model tends to underestimate phytoplankton during the bloom peak, and produces a delayed fall bloom in the northern bins. A fall bloom, which is not present in the observations, is also simulated in the southern bins. Aside from differences in the fall concentrations, the development of the spring bloom and the annual cycle of phytoplankton are captured remarkably well in the individually and jointly optimized models, especially when considering the model's simplicity. The model also captures other aspects of real plankton communities such a subsurface phytoplankton biomass maximum during summer (Fig. 1E) and the spatial increase in average phytoplankton concentrations from southern to northern bins (Fig. 2, Appendix A). Simulated zooplankton concentrations are very low in winter, start increasing rapidly in April and peak about the same time as phytoplankton, matching or exceeding phytoplankton concentrations. Zooplankton then decreases in parallel with phytoplankton from June to October and remains low throughout winter. Unfortunately no observations specific to the area can be directly used to validate or constrain parameters of the zooplankton functional group in our model (i.e., a combination of micro- and mesozooplankton). Because they are limited to larger species, zooplankton estimates from Continuous Plankton Recorder observations are better used to qualitatively validate models with a separate mesozooplankton group (e.g., Lewis et al., 2006). Nonetheless, our zooplankton cycles agree qualitatively with the annual cycle of copepod abundances in the area (Colebrook, 1979).

The individually optimized models replicate the observed Day^{P*} accurately with an average bias of 7.8 days (Table 3, Fig. 2); that is, according to the biomass threshold method, the simulated bloom initiation precedes the observed by about a week. The second metric Day^{r*} is also accurate, exhibiting an average bias of 4.3 days. In our simulations, positive accumulation rates occur during winter as in the observations (Fig. 3, Table 3), which is a key criticism of the critical depth hypothesis. In comparison to the individually optimized results, slightly larger misfits are observed using the jointly optimized parameters, especially with respect to Day^{P*} and Day^{r*} (Table 3). For that reason we choose to use the individually optimized parameters throughout the remainder of the manuscript.

3.2. Optimal parameter values

The individually optimized parameters show spatial differentiation between northern and southern bins (Fig. 4), mainly driven by the parameter values of detrital sinking (w_D), grazing rate (μ_{max}), the nutrient uptake half-saturation (k_N), and the phytoplankton growth parameter (μ_0). The first and second principal components (PC1 and PC2) explain 87% and 6.4% of the variance among parameter sets. The parameter w_D explains 98% of PC1 and 15% of PC2 (85% of total variance); μ_{max} explains 11% of PC1 and 75% of PC2 (7% of total variance); k_N explains 9% of PC1 and 62% of PC2 (6.8% of total variance); and μ_0 explains 6% of PC1 and 15% of PC2 (0.6% of total variance). The parameter w_D is higher in the southern bins, whereas g_{max} and μ_0 are higher in the northern bins. k_N does not vary consistently with latitude. As northern and southern bins are different in terms of light, mixed layer depth,

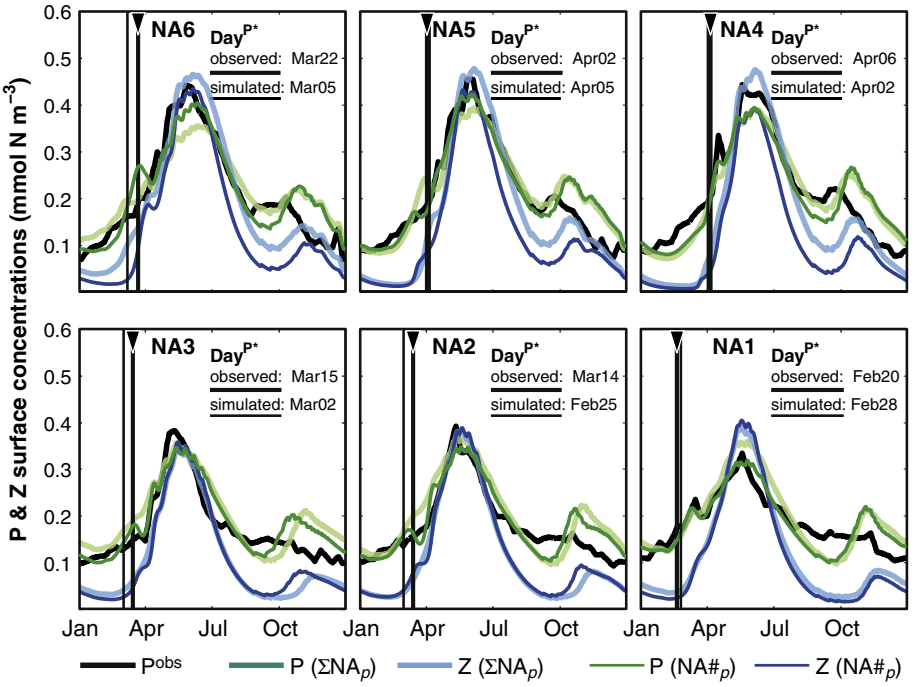

Fig. 2. Comparison between satellite-based phytoplankton biomass (P^{obs}) and daily averaged simulated phytoplankton using jointly ($\sum NA_p$) and individually ($NA\#_p$) optimized parameters. The solid vertical lines mark the day of bloom initiation according to the biomass based metric Day^{P^*} in the observations (thick line with inverted triangle on top) and individually optimized simulations (thin line).

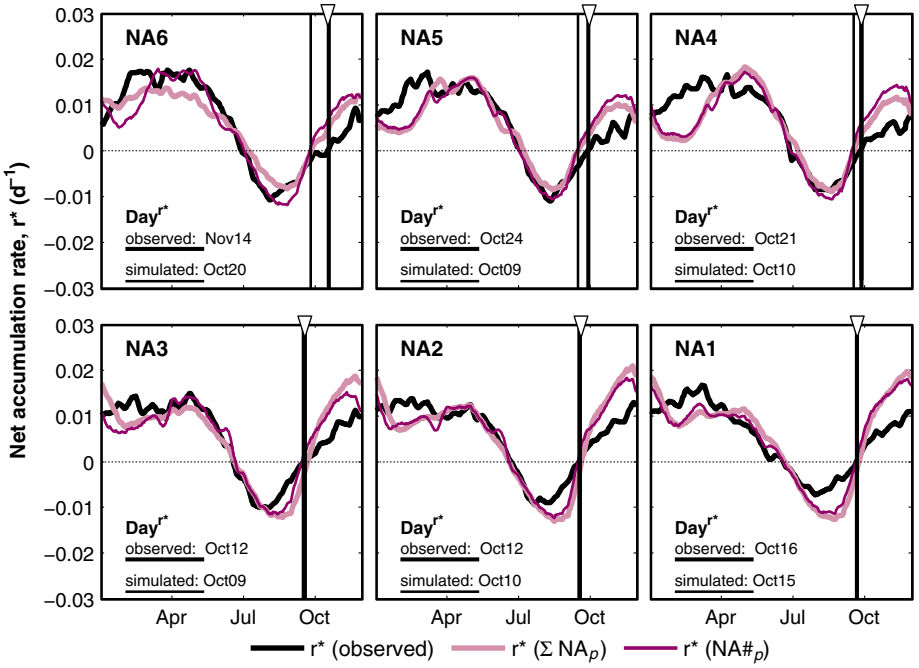

Fig. 3. Phytoplankton inventory net accumulation rates, r^*, estimated from the phytoplankton biomass observations (black line) and from the simulations using jointly ($\sum NA_p$, thick pink line) and individually ($NA\#_p$, thin purple line) optimized parameters. The solid vertical lines mark the day of bloom initiation according to the accumulation rate metric (Day^{r^*}) in the observations (thick line with inverted triangle on top) and individually optimized simulations (thin line). In the bottom panels the thick and thin vertical lines coincide. (For interpretation of the references to color in this figure legend, the reader is referred to the web version of this article.)

nutrient and chlorophyll regimes (Henson et al., 2009), it is not unreasonable to think that the differences in parameter values reflect these features (Appendix A). It is important to reiterate that despite the small spatial differences in these parameters, model solutions using the jointly optimized parameter set $\sum NA_p$ are very similar to the individually optimized ones (Tables 2 and 3; Figs. 2 and 3).

Overall, the algorithm favored optimal values of μ_0 between 0.6 d^{-1} and 1 d^{-1}. Accounting for the effect of temperature dependency on phytoplankton growth, realized maximum growth rates (μ_{max}), are within the range of observed values (Fahnenstiel et al., 1995; Sarthou et al., 2005). For example, in bin N5 μ_{max} ranges between 1.48 d^{-1} and 2.46 d^{-1} given temperatures between 10 °C and 18 °C. The phytoplankton metabolic loss and mortality rates

Table 2
Optimal parameters resulting from individual and jointly optimizations. The variance (σ^2) of optimal parameters with respect to all bins and the joint optimization is shown as a reference of spatial differences in parameter values. The cost value (F), root mean square error (RMSE) and goodness of fit (r^2) are shown as metrics comparing the performance of simulated surface phytoplankton with respect to satellite-based phytoplankton biomass.

	NA1	NA2	NA3	NA4	NA5	NA6	$\sum NA$	σ^2
α	0.1149	0.1472	0.1115	0.1835	0.2099	0.1249	0.1953	0.0017
μ_0	0.9174	0.9280	0.9918	0.5976	0.7894	0.6548	0.6989	0.0232
k_N	2.4856	2.0795	1.7406	2.1135	3.4151	2.3549	2.3868	0.2754
g_{max}	3.4191	2.6684	2.4796	2.1533	2.0811	1.8010	2.1522	0.2832
K_P^2	0.8048	0.5208	0.5012	0.5109	0.5373	0.5470	0.5573	0.0113
β	0.9108	0.9178	0.9169	0.8038	0.8781	0.9463	0.9116	0.0021
l_{PN}	0.0065	0.0061	0.0094	0.0052	0.0062	0.0088	0.0066	0.0000
l_{PD}	0.0116	0.0124	0.0124	0.0102	0.0109	0.0109	0.0101	0.0000
l_{ZN}	0.0191	0.0109	0.0102	0.0193	0.0133	0.0102	0.0102	0.0000
l_{ZD}	0.2757	0.3948	0.3984	0.3693	0.3998	0.3954	0.3395	0.0021
r_{DN}	0.1217	0.1490	0.1218	0.1402	0.1401	0.1455	0.1213	0.0001
w_D	4.3870	2.7667	2.2903	6.9805	5.0400	6.3737	2.7489	3.4671
w_P	0.1260	0.1279	0.1115	0.1330	0.1117	0.1118	0.2551	0.0027
F	0.4095	0.3800	0.5840	0.8760	0.5475	0.8395	5.3290	–
RMSE ($NA\#_p$)	0.0313	0.0308	0.0334	0.0446	0.0354	0.0405	–	–
RMSE ($\sum NA_p$)	0.0409	0.0406	0.0429	0.0406	0.0383	0.0455	–	–
r^2 ($NA\#_p$)	0.75	0.84	0.84	0.83	0.90	0.85	–	–
r^2 ($\sum NA_p$)	0.75	0.80	0.78	0.85	0.88	0.89	–	–

Table 3
Spring bloom initiation metrics estimated using the satellite-based phytoplankton biomass (P^{obs}), and simulated surface phytoplankton using individually optimized parameters ($NA\#_p$) for each bin, and jointly optimized parameters ($\sum NA_p$) for all bins. Day^{P*} is the biomass-based metric and Day^{r*} is the metric based on the phytoplankton inventory accumulation rate.

	Day^{P*}			Day^{r*}		
	P^{obs}	$NA\#_p$	$\sum NA_p$	P^{obs}	$NA\#_p$	$\sum NA_p$
NA1	52	57	51	290	289	293
NA2	74	60	57	286	284	290
NA3	75	62	52	286	283	292
NA4	97	95	93	294	284	286
NA5	93	96	75	298	283	286
NA6	82	68	61	319	294	296

consistently show a tendency toward the lower limit imposed in the optimization. The excretion rate of zooplankton also tends toward low values, whereas the zooplankton mortality rates and assimilation efficiency tend toward values at the upper limit (Table 2). Although these estimates are close to those applied in other ecosystem models, the algorithm's behavior may be influenced by the limited availability of observations (Schartau and Oschlies, 2003). A detailed discussion of these tendencies is outside the scope of this manuscript and may distract from the objectives of this analysis. Nevertheless, as experimental results may be influenced by the choice of parameter values, it is important to estimate how they affect the model response.

By analyzing the model sensitivity to doubling and halving each optimized parameter value (Fig. 5), we observe that w_D has a negligible impact on the phytoplankton annual cycle, which explains why ΣNA_p parameters are able to fit all observed cycles despite differences in this parameter (Fig. 4). Most interestingly, we find that parameters that primarily affect the phytoplankton formulation (α, μ_0, k_N, w_P, l_{PN}, l_{PD}) modify the shape of the climatological annual cycle, and affect the slope of bloom development and thus timing of the bloom. In particular, the model is highly sensitive to changes in μ_0; doubling its value produces an earlier increase in phytoplankton, while halving it produces a delayed and more abrupt bloom. The opposite effect is observed when modifying the loss rates l_{PN} and l_{PD}. Parameters that directly affect grazing (g_{max}, k_P, β, l_{ZN}, l_{ZD}) modify the average phytoplankton concentrations throughout the year, but mostly preserve the shape of the phytoplankton annual cycle. Phytoplankton is not sensitive to changes in zooplankton excretion (l_{ZN}), and only sensitive to zooplankton mortality (l_{ZD}) during summer.

3.3. Model sensitivity to variables

Results of the analysis of model sensitivity to perturbations in physical and biological variables (Fig. 6) show that independent perturbations (i.e., 1st derivative) of light, zooplankton and temperature result in the strongest effects on phytoplankton surface concentrations in spring, when increases in light and temperature lead to increases in phytoplankton, while increases in zooplankton lead to a decrease. Perturbations in light and temperature affect predominantly the surface, while zooplankton perturbations affect the entire water column. As nutrients are abundant during winter and spring, perturbing N only affects phytoplankton in summer and fall. Locally, changes produced by perturbing H_{MLD} can be up to two orders of magnitude greater than those that result from perturbing the other variables, but they only act to redistribute concentrations within the water column. The vertically integrated change in phytoplankton produced by perturbing the mixed layer is negligible ($<10^{-10}$ mmol N m^{-2}) when compared against vertically integrated changes produced by perturbations in all other variables (Fig. 6F). When comparing the absolute vertically integrated values, we notice that for the given set of optimized parameters the model is most sensitive to light and zooplankton, where the model's sensitivity to light is the larger of the two terms for most of the year. When the second derivative terms are added (solid lines in Fig. 6F), the overall effect of light is slightly decreased, but is still significantly higher than the effect of zooplankton during winter. The effect of perturbing zooplankton is equivalent in magnitude to the effect of perturbing light during April, at the time when the shoaling of the H_{MLD} and the highest phytoplankton accumulation rates occur.

4. Experimental simulations

4.1. Experiment I: zooplankton response to a shoaling mixed layer

Early experiments with an idealized 0D model by Evans and Parslow (1985) examined how simulated phytoplankton annual cycles were influenced by seasonal fluctuations of the mixed layer.

Table 4
Brief description of the idealized experiment configurations and main conclusions.

Experiment	Treatment	Conclusions
Exp. I. Zooplankton accumulation mechanism (i.e., entrainment): – Modified Eq. (4) – Section 4.1 – Fig. 7	Accumulation mechanism term added to Eq. (4)	Effects of zooplankton entrainment over phytoplankton are small Zooplankton response is dominated by food availability
Exp. II. Constant mixed layer depth: – No seasonal fluctuations of mixed layer – 10 years experimental conditions – Section 4.2 – Fig. 8	a. Constant H_{MLD} = max (H_{MLD}) b. Constant H_{MLD} > max (Euphotic depth) c. Constant H_{MLD} > min (Euphotic depth) d. Constant H_{MLD} = min (H_{MLD})	Shoaling of the mixed layer enhances phytoplankton growth by improving light conditions; as long as the shoaling does not compromise nutrient availability or phytoplankton residence time within the mixed layer Zooplankton response is dominated by food availability
Exp. III. Part 1: Constant zooplankton biomass, varying total zooplankton concentrations: – Disrupted *P* to *Z* feedback – Climatological H_{MLD} – 10 years experimental conditions – Section 4.3 – Fig. 9A–E	a. Low zooplankton biomass (Z_{total} = 5 mmol N m^{-2}) b. High zooplankton biomass (Z_{total} = 10 mmol N m^{-2})	Lower zooplankton biomass produces higher phytoplankton biomass overall Changes in bloom initiation are small because the same nutrient level is available
Exp III. Part 2: Constant zooplankton biomass, varying winter zooplankton dilution levels by changing winter mixed layer depth: – Disrupted *P* to *Z* feedback – Idealized H^*_{MLD} with varying maximum winter depths – 10 years experimental conditions – Section 4.3 – Fig. 9F–J	a. Low zooplankton biomass ($\max(H^*_{MLD})$ = $\max(H_{MLD})$) b. High zooplankton biomass ($\max(H^*_{MLD})$ = 25 m)	Shallow winter mixed layers produce increased winter phytoplankton biomass and accumulation rates despite high grazing rate and decreased nutrient availability Shallow winter mixed layers enhance phytoplankton growth by improving light conditions

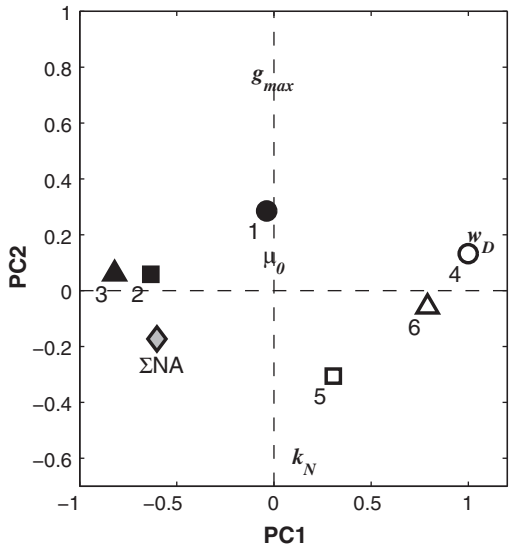

Fig. 4. Results of the principal component analysis of optimized parameters, showing the scaled arrangement of optimized parameter sets projected onto the first and second principal component (PC1, PC2). Solid black symbols represent parameter sets for the southern bins ($\sum NA_pNA1_p$ to $NA3_p$), empty symbols are for the northern bins ($NA4_p$–$NA6_p$), and the gray diamond corresponds to the jointly optimized parameter set ($\sum NA$). The distance between their symbols is representative of how different the parameter sets are. The location of the symbols w_D, g_{max}, k_N, μ_0 represents the scaled contribution of these parameters to the variance explained by PC1 and PC2.

When conceptualizing their model, they postulated that phytoplankton and zooplankton respond asymmetrically to the shoaling of the mixed layer assuming that a deepening mixed layer equally dilutes both types of organisms, but that a shoaling of the mixed layer would affect motile zooplankton by concentrating them in the mixed layer while a fraction of the relatively motionless phytoplankton would remain below the mixed layer. This asymmetric response to a shoaling mixed layer is in line with the dilution-recoupling hypothesis, in the sense that the physically driven accumulation of zooplankton contributes to the recoupling of the planktonic prey–predator relationship (Behrenfeld, 2010). However, Evans and Parslow also showed that spring blooms can occur in the absence of mixed layer fluctuations (see Section 4.2), which argues against the shoaling of the mixed layer as a mechanism for spring bloom initiation, and indirectly dismisses the asymmetric response as a process involved in seasonal bloom dynamics. Furthermore, motile zooplankton may stay below the mixed layer to follow their prey, instead of tracking the mixed layer shoaling, because non-motile phytoplankton is not concentrated during the shoaling.

In order to verify whether the hypothetical accumulation of zooplankton in response to a shoaling mixed layer has any effect on phytoplankton annual cycles in our model, we followed Evans and Parslow's formulation of the mechanism by introducing the zooplankton accumulation term $\xi = -\frac{1}{H_{MLD}}\frac{dH_{MLD}}{dt}Z$ on the right hand side of Eq. (2), and allowing it to take effect only when the mixed layer shoals, i.e., $\frac{dH_{MLD}}{dt} < 0$. We expect a noticeable direct effect on zooplankton concentrations in the surface mixed layer and an indirect one on phytoplankton only if the term ξ is significant in comparison to the zooplankton growth rate (i.e., the first term in Eq. (2)). The ratio of these two terms, the non-dimensional number $\frac{\xi}{Z\beta g}$, is plotted in Fig. 7A for a preliminary inspection of the potential effects of the zooplankton concentrating mechanism. High values of this number would indicate that the accumulation of zooplankton driven by the mixed layer shoaling contributes significantly to total biomass changes in the mixed layer, a condition that can only occur at low βg (i.e., low phytoplankton concentrations) and high $\frac{\xi}{Z}$ (i.e., small H_{MLD} and a rapidly shoaling mixed layer). The black dots in Fig. 7A show that high values of $\frac{\xi}{Z\beta g}$ do not occur at any time throughout year $\left(\frac{\xi}{Z\beta g}\right.$ is always smaller than 0.3$\left.\right)$.

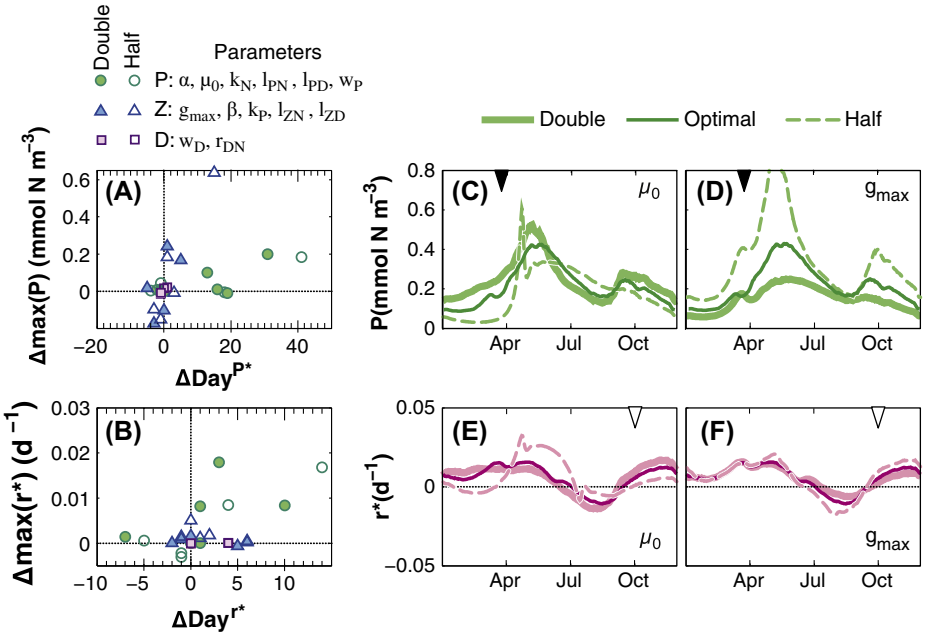

Fig. 5. Sensitivity of the simulated surface phytoplankton biomass (P) and inventory accumulation rate (r^*) to halving (empty symbols) and doubling (filled symbols) optimal parameter values, exemplified by results in bin NA5. (A) and (B) show the change in the date of bloom initiation according to the biomass-based metric (ΔDay^{P*}) and the accumulation rate metric (ΔDay^{r*}), as well as the change in maximum phytoplankton biomass and accumulation rates ($\Delta \max(P)$ and $\Delta \max(r^*)$, respectively). Different symbols are used to represent the biological variable each parameter primarily modifies (i.e., phytoplankton (P, green circles), zooplankton (Z, blue triangles) or detritus (D, purple squares)). These values were obtained by comparing the optimized results against the sensitivity tests (i.e., test minus optimized simulation). Subplots (C)–(F) show how the temporal evolution of phytoplankton biomass and net phytoplankton accumulation rate responds to variations in parameters μ_0 and g_{max}. As a reference, the inverted triangles on top of the x-axes show the date of bloom initiation in the observations according to the biomass-based metric (black, (C) and (D)) and the metric based on the accumulation rate (white, (E) and (F)). (For interpretation of the references to color in this figure legend, the reader is referred to the web version of this article.)

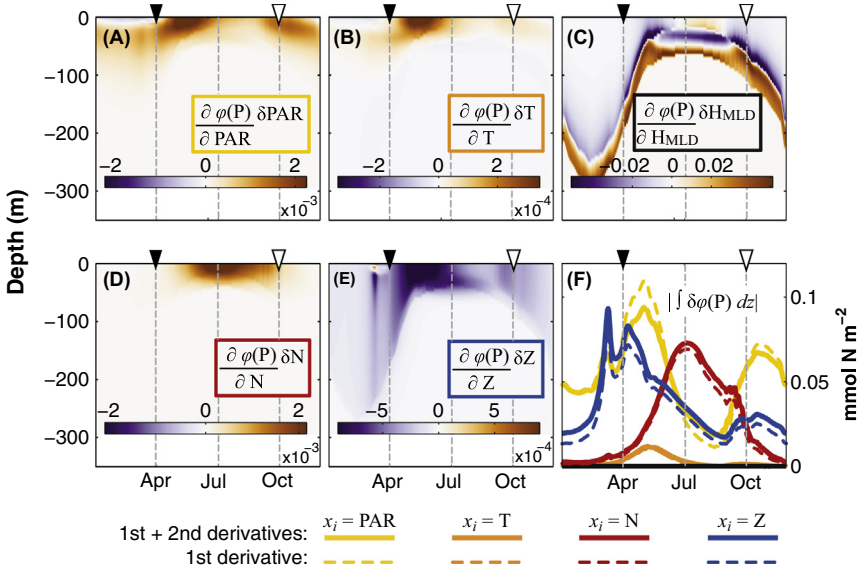

Fig. 6. Phytoplankton sensitivity to small perturbations in physical and biological variables, using a 2nd order Taylor approximation. The surface subplots show the first order phytoplankton response to perturbations in (A) photosynthetic active radiation; (B) temperature; (C) mixed layer depth; (D) nutrient; and (E) zooplankton. Subplot (F) shows the absolute vertically integrated 1st (dashed) and 1st + 2nd (solid) order terms of the Taylor approximations. The vertically integrated effect of perturbations to the mixed layer is negligible, as changes above and below the mixed layer offset each other. As a reference, the inverted triangles on top of the x-axes show the date of bloom initiation in the observations according to the biomass-based metric (black) and the metric based on the accumulation rate (white).

When the zooplankton accumulation mechanism is added to the model, only small differences in phytoplankton and zooplankton concentrations are observed. For instance, the metrics of bloom initiation change only by up to 2 days (Table 4). Percentage changes in phytoplankton and zooplankton (Fig. 7B) were evaluated by comparing model results with and without the additional term in the zooplankton equation $\left(\frac{\text{Experiment}-\text{Optimized}}{\text{Optimized}} \times 100\right)$. The mechanism produces a 10% increase in zooplankton concentrations between March and April; however, as zooplankton concentrations are very low during these months, the change in zooplankton concentration translates into a ~7% decrease in surface phytoplankton

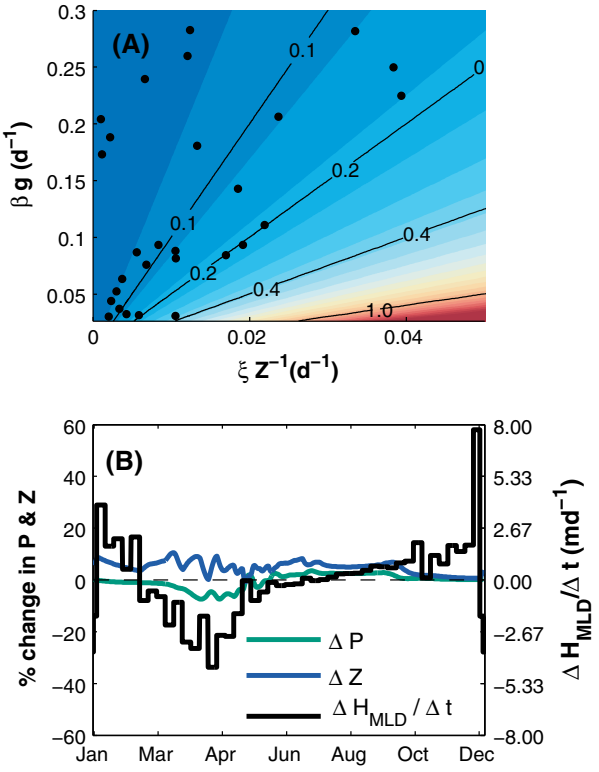

Fig. 7. (A) Relative contribution of the accumulation of zooplankton biomass due to a shoaling mixed layer (ξZ^{-1}) over changes in zooplankton biomass due to assimilated grazing (βg) in bin NA5. Black dots show actual values of the non-dimensional number $\frac{\xi}{Z\beta g}$ from the optimized annual cycles, subsampled every 4 days. (B) Annual cycle of changes in the mixed layer ($\frac{\Delta H_{MLD}}{\Delta t}$, black line) and percentual change in simulated surface phytoplankton (green line) and zooplankton (blue line) concentrations caused by the application of an explicit zooplankton response to the mixed layer shoaling. (For interpretation of the references to color in this figure legend, the reader is referred to the web version of this article.)

during the peak of the spring bloom and a 3% increase of fall concentrations. This suggests that although the active zooplankton response to a shoaling mixed layer is plausible and does affect phytoplankton biomass and accumulation rates, it is not a major contributor to changes in the community phenology of the Subpolar North Atlantic as portrayed in our model.

4.2. Experiment II: system response in the absence of mixed layer fluctuations

We address another of Evans and Parslow's considerations, which had implications for the critical-depth paradigm: the development of blooms in the absence of mixed layer fluctuations, Specifically, we present results obtained by setting the mixed layer depth as constant year-round at its minimum and maximum climatological values (e.g., 16 m and 249 m for NA5). We also use two intermediate constant mixed layers (50 and 25 m), which are shallower than the annual maximum but deeper than the maximum and minimum euphotic zone depth, respectively. The euphotic zone depth is defined as the depth at which light limitation for phytoplankton growth is lower than 1% ($Lim_I < 1\%$). For the experiments, the model is initialized with the distribution of state variables resulting from the optimized simulations and forced with a constant H_{MLD} for 10 years. Nutrient nudging ($\gamma = \frac{1}{30}$) is limited to the bottom 15 m, as it would otherwise introduce dynamics similar to a time varying mixed layer.

When analyzing the resulting spring bloom initiation according to both metrics (Fig. 8A and B), we observe that the constant mixed layers which were shallower than the minimum euphotic zone (25 and 16 m) produced delayed blooms in comparison with the one obtained with a very deep mixed layer. In contrast, the treatment with a mixed layer of 100 m produced the earliest of the blooms (Fig. 8A and B). These patterns can be better understood when observing the conditions during the initial years of the experimental runs (Fig. 8C–E). When experimental conditions are first enforced, all simulations have non-limiting nutrient conditions. All experimental mixed layers shallower than the maximum produce an immediate abrupt increase in phytoplankton concentrations followed by an increase in zooplankton. This abrupt increase in biomass can be explained by improved light conditions. Over time, the shallower mixed layer depths (i.e., 100, 25 and 16 m) inhibit an effective injection of nutrients to the surface, resulting in year-round low-nutrient concentrations within the mixed layer (Fig. 8E). Phytoplankton growth can still occur below these shallow mixed layers, where nutrients and light are available, but the stagnant bottom layer allows phytoplankton to sink rapidly (Lande and Wood, 1987). The combined effect of surface nutrient depletion and aggravated sinking losses diminishes phytoplankton surface concentrations and delays the bloom initiation according to both Day^{P*} and Day^{r*} metrics in the 25 m and 16 m mixed layer cases. Nonetheless, the constant 100 m mixed layer is able to improve phytoplankton exposure to light, without significantly increasing its sinking losses and thus, over time, it maintains higher biomass than the deepest mixed layer case.

We can therefore generalize that a shoaling of the mixed layer enhances phytoplankton growth by improving light conditions; this may result in an increase in phytoplankton biomass and accumulation rates, as long as the shoaling does not compromise nutrient availability or phytoplankton residence time within the mixed layer.

4.3. Experiment III: effects of zooplankton dilution and concentration

Results of experiments I and II demonstrate that food availability dominates the zooplankton response in the model (Figs. 6 and 7D). To avoid that dominant response, in this experiment we intentionally disrupted the bottom-up feedback from phytoplankton to zooplankton by directly prescribing different zooplankton biomasses in the mixed layer. Therefore, this experiment goes a step further than the zooplankton concentrating experiment (experiment I) in terms of testing the dilution-recoupling mechanism. It is possible that in experiment I winter zooplankton concentration is lower than in reality and thus the effect of dilution/recoupling is not as strong as it should be. By artificially imposing zooplankton, here we circumvent this issue and directly test whether a deepening/shoaling of the mixed layer creates large enough changes in grazing pressure to significantly affect phytoplankton concentrations. By prescribing a constant, vertically integrated zooplankton biomass (Z_{total} in mmol N m^{-2}) in the mixed layer, H_{MLD} effectively dilutes and concentrates zooplankton (Z in mmol N m^{-3}) in these simulations (see schematic of the experiment in Fig. 10A). We aim to answer whether and how these physically driven changes in zooplankton concentrations affect the timing of the phytoplankton spring bloom according to our two timing metrics. Again all experiments were run for 10 years.

The resulting cycles illustrate that the amount of zooplankton diluted in the mixed layer influences phytoplankton concentrations (Fig. 9A and C) and accumulation rates (Fig. 9B) in a similar fashion as modifying zooplankton parameters did (Fig. 5): the main change is in the magnitude of the bloom, with small shifts in timing. When low Z_{total} is present in the mixed layer, the phytoplankton bloom peak is larger than in the case with high Z_{total}. In both cases, the peak is significantly larger than in the observations,

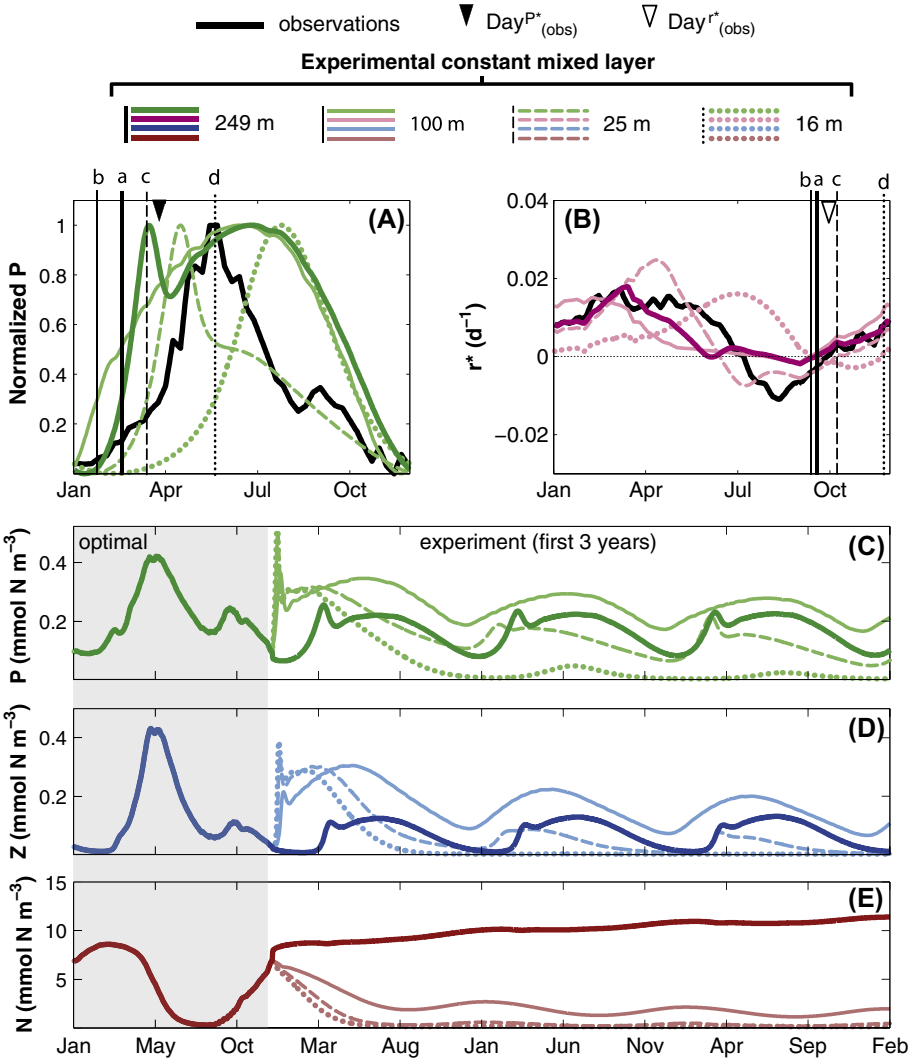

Fig. 8. Results of Experiment II in bin NA5: model runs during 10 years using constant mixed layer depths equal to a. 249 m (maximum time varying H_{MLD}), b. 50 m (below maximum euphotic depth), c. 25 m (below minimum euphotic depth), and d. 16 m (minimum time varying H_{MLD}. (A) Normalized satellite-based phytoplankton biomass ("observations") and simulated surface phytoplankton of the last experimental cycle, used to determine the date of bloom initiation according to the biomass based metric (Day^{P^*}). (B) Net phytoplankton accumulation rate estimated from "observations" and experimental simulations of the last experimental cycle, used to determine the date of bloom initiation according to the rate metric (Day^{r^*}). Vertical lines in (A) and (B) respectively mark Day^{P^*} and Day^{r^*} in each experiment, while the inverted triangles at the top *x*-axes mark Day^{P^*} and Day^{r^*} in the observations as a reference. (C), (D) and (E), show the corresponding surface phytoplankton, zooplankton and nutrient optimal cycles and the first 3 annual cycles of experimental conditions.

and a Z_{total} as large as 20 mmol N m^{-2} would be needed to produce a bloom peak of similar magnitude as the observations. In the scenario with high Z_{total}, zooplankton concentrations effectively keep the growth of phytoplankton in check, resulting in lower winter phytoplankton, a smaller bloom peak, and a shorter bloom.

The bloom initiation metrics have opposite patterns in this experiment. Low Z_{total} produces an earlier Day^{P*} than high Z_{total}, but a delayed Day^{r*}. That is, the biomass-based bloom initiation metric pattern agrees with the dilution-recoupling hypothesis (i.e., lower zooplankton = earlier bloom); but the metric based on the accumulation rate, which was used to develop the hypothesis, does not. Somewhat counter-intuitively, high zooplankton biomass during summer not only decreases phytoplankton biomass through heavy grazing, but also increases phytoplankton growth rates by providing recycled nutrients through excretion. The change in Day^{P*} by doubling Z_{total} from 5 to 10 mmol N m^{-2} is only 8 days in bin NA5 (6.3 days on average for all bins). There are larger differences in the bloom initiation date according to Day^{r*} (16 days in bin NA5, and 13.6 days on average for all bins), but given that it behaves opposite to what was envisioned by the dilution-recoupling hypothesis, we consider that neither of the bloom timing metrics supports the idea that an increase in winter zooplankton biomass, decoupled from ecosystem feedbacks, can significantly delay the spring bloom; i.e., more zooplankton does not necessarily produce a delayed bloom, but a smaller one. As seen in Fig. 5D and F, phytoplankton biomass in the model appears to be more sensitive to changes in zooplankton parameters than the accumulation rates.

As the dilution-recoupling hypothesis discusses variations in grazing forced by the mixed layer deepening, in a new set of experiments we use equal values of constant zooplankton biomass to evaluate the effect of different winter dilution levels independently (Fig. 9F–J). In these experiments, we configure Z_{total} = 10 mmol N m^{-2} as constant within the mixed layer and vary the maximum depth of the mixed layer annual cycle (249 m and 25 m, in Fig. 9). For this purpose, we define an idealized climatological evolution of the mixed layer depth, H^*_{MLD}, that allows us to control maximum depth values while preserving the minimum summer values in all cases, such that zooplankton concentrations are equal during summer, but diluted to different concentrations

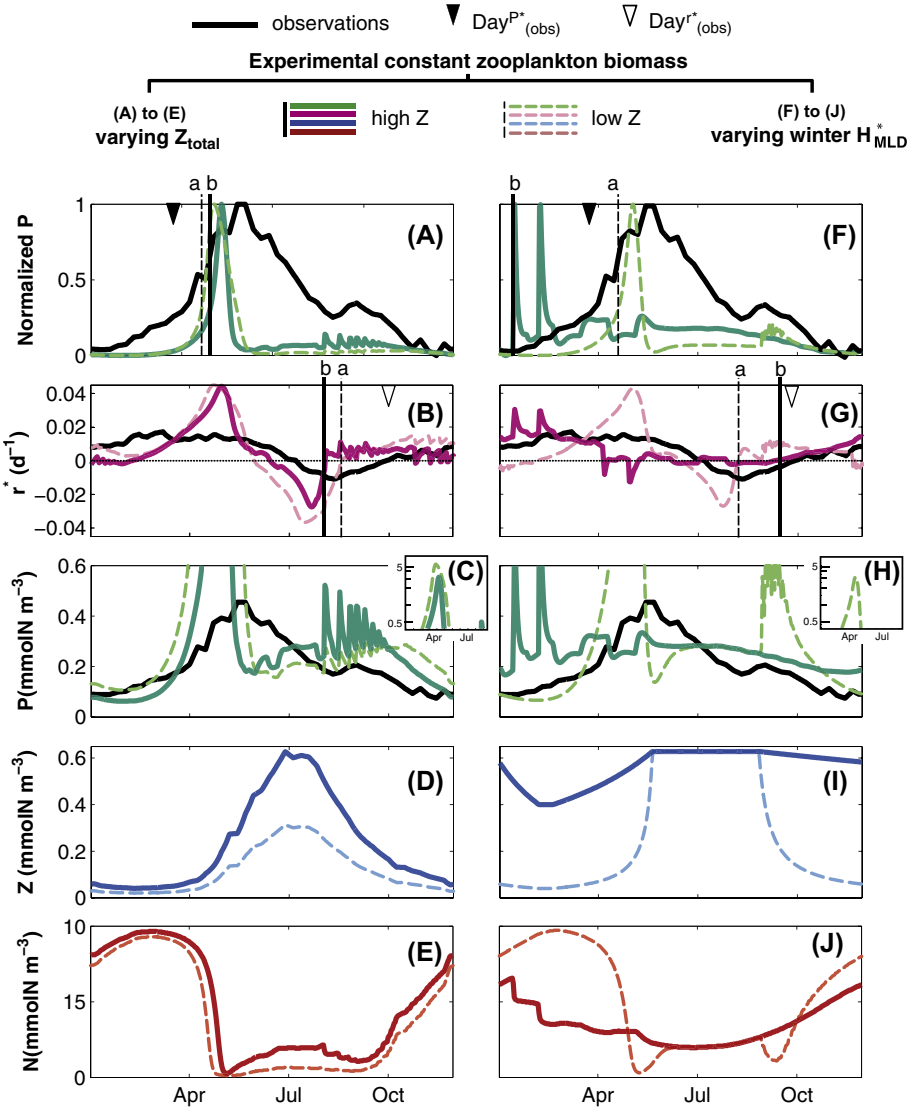

Fig. 9. Results of Experiment III in bin NA5: constant zooplankton biomass experiments in bin NA5 after 10 years of experimental conditions. Subplots (A) to (E) use the prescribed mixed layer annual cycle in H_{MLD}, but prescribe the total amount of zooplankton in the mixed layer such that: a. "low Z" refers to Z_{total} = 5 mmol N m^{-2} and b. "high Z" to Z_{total} = 10 mmol N m^{-2}. Subplots (F) to (J) use Z_{total} = 10 mmol N m^{-2} and the idealized mixed layer annual cycle H^*_{MLD} to compare results with different winter mixed layer depths, as a proxy to impose different winter dilution levels to zooplankton: a. "low Z" is achieved with max(H^*_{MLD}) = 249 m and b. "high Z" uses max(H^*_{MLD}) = 25 m. (A) and (F) Normalized phytoplankton satellite-based biomass ("observations") and simulated surface phytoplankton of the last experimental cycle, used to determine the date of bloom initiation according to the biomass based metric (Day^{P^*}). (B) and (G) Net phytoplankton accumulation rate estimated from "observations" and experimental simulations of the last experimental cycle, used to determine the date of bloom initiation according to the rate metric (Day^{r^*}). Vertical lines in the normalized P and r^* subplots mark the date of bloom initiation according to the biomass and rate based metrics (Day^{P*} and Day^{r*}, respectively) in the experiments. The inverted triangles at the top x-axes mark Day^{P^*} and Day^{r^*} in the observations, as a reference. (C) and (H) show the corresponding phytoplankton satellite-based biomass ("observations") and simulated surface phytoplankton of the last experimental cycle. (D), (I) and (E), (J) show the corresponding surface zooplankton and nutrient annual cycles, respectively.

as the mixed layer deepens. H^*_{MLD} is similar to that of Evans and Parslow (1985) and replicates the timing of deepening and shoaling of the climatological mixed layer depth used in the optimized simulations (Fig. 9A).

Based on the dilution-recoupling hypothesis, deeper winter mixing would be expected to produce early positive accumulation rates that translate into an early spring bloom. The bloom initiation metric based on accumulation rate, Day^{r*}, supports this theoretical behavior. The first positive accumulation rates for shallow winter mixing occur later than for deep winter mixing (Day^{r*} = 358 and 278, respectively); but rates in the shallow winter mixing case are consistently increasing from October onward and exceed those obtained in winter for the case with deep winter mixing (Fig. 9G). In terms of phytoplankton biomass (Fig. 9F and H), the bloom appears to initiate earlier when the winter mixed layer is shallow (Day^{P*} = 15 for a winter mixed layer of 25 m, compared to Day^{P*} = 120 when using 249 m). This occurs as the intermediate mixed layer depth of 25 m maintains phytoplankton in the upper ocean layers and exposes them to better light conditions during winter, allowing high positive growth rates despite low incoming light and high grazing. In coherence with the results of the constant mixed layer experiment, here the shallow winter mixed layer hinders annual nutrient replenishment (Fig. 9J) and determines the upper limit of phytoplankton concentrations.

We tested 450 combinations of winter H^*_{MLD} and Z_{total} and compare the results in terms of Day^{P*} and Day^{r*} (Fig. 10B and C). The response is non-linear; however, it reproduces the same conclusions derived from Fig. 9: when the bloom initiation is estimated using the biomass-based metric (Day^{P*}), deep winter dilution produces a late bloom initiation, shallow dilution an early one

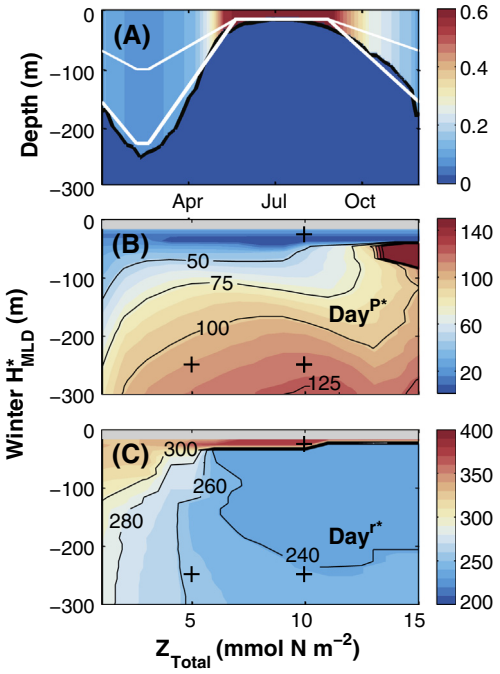

Fig. 10. (A) Scheme of Experiment III: shows a constant zooplankton biomass Z_{total} = 10 mmol N m^{-2} prescribed in the mixed layer, being diluted and concentrated by the climatological mixed layer depth H_{MLD} (black). Zooplankton concentrations below the mixed layer are 0 mmol m^{-3}. White lines show examples of the idealized mixed layer, H^*_{MLD}, with two different winter values: 100 m and 225 m. (B) Date of bloom initiation according to the biomass-based metric Day^{P*}, in Julian days. (C) Date of bloom initiation according to the accumulation rate-based metric Day^{r*}, in Julian days. The symbol "+" in (B) and (C) marks Z_{total} versus the max(H^*_{MLD}) conditions used in Fig. 9. Winter mixed layers shallower than the climatological minimum were not tested (gray background).

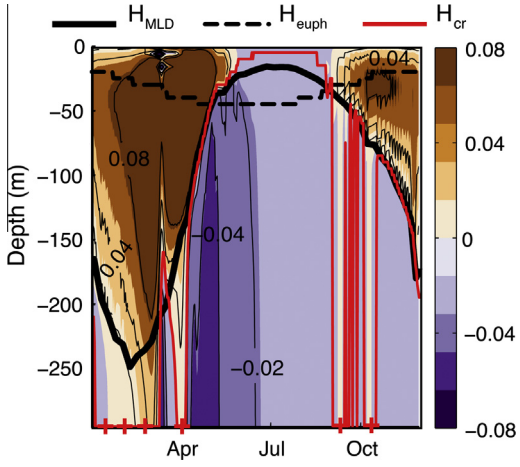

Fig. 11. Vertically integrated phytoplankton growth minus vertically integrated phytoplankton losses as function of integration depth calculated downward from the surface (i.e., $R(z,t)$ in Eq. (9)), for bin NA5. The critical depth (H_{cr}) is found where $R(z,t)$ = 0, which lies deeper than the mixed layer depth (H_{MLD}) prior to the spring and fall blooms. The critical-depth criterion for bloom initiation ($H_{cr} > H_{MLD}$) is therefore satisfied. Red + symbols denote periods when the critical depth is deeper than the model domain. H_{euph} marks the depth of the euphotic zone as a reference. (For interpretation of the references to color in this figure legend, the reader is referred to the web version of this article.)

(Fig. 9B). This is opposite to what one would expect if physical decoupling of phytoplankton growth and grazing had a major effect on the spring bloom onset. When the phytoplankton inventory accumulation rates are considered (Day^{r*}), the changes in bloom initiation due to changes in winter mixed layer depth are coherent with the dilution-recoupling mechanism; however, shifts in timing are only significant when the winter mixed layer is shallow (winter $H^*_{MLD} < 100$ m) and when zooplankton biomass is very low (Z_{total} = 5 mmol N m^{-2}). This agrees with the results of experiment I (Section 4.1) and suggests that a different regime exists where physical dilution of zooplankton is a significant factor determining the bloom initiation. This different regime may be exemplified by subtropical areas and High-Nutrient–Low-Chlorophyll areas with a shallow winter mixed layer. These areas are characterized by small phytoplankton sizes, and low and rather constant biomass, where grazing is recognized as an important control (Fasham et al., 1990; Miller et al., 1991; Steele and Henderson, 1992).

5. Discussion

5.1. Is the optimized model consistent with the critical-depth hypothesis?

Our optimized model results replicate observations with positive phytoplankton inventory accumulation rates starting in late autumn and throughout winter (Table 3, Fig. 3); the inability of the critical-depth hypothesis to explain positive net accumulation is one of its most frequently reiterated criticisms. In discussing our results, we distinguish two key aspects of the critical-depth hypothesis: (1) the bloom initiation criterion and (2) the critical-depth model.

The bloom initiation criterion simply states that "blooming can occur only if the depth of the mixed layer is less than the critical value" (Sverdrup, 1953). This critical depth value has been calculated with the help of analytical models (e.g., Siegel et al., 2002; Sverdrup, 1953; Platt et al., 1991) as the depth where the vertically integrated phytoplankton production is matched by the vertically integrated phytoplankton "destruction" by respiration. If the term "destruction", used by Sverdrup (1953), is assumed to include all community losses, mixing and sinking, rather than only phytoplankton metabolism (Smetacek and Passow, 1990), the critical depth (H_{cr}) at any point in time can be found directly from our vertically resolved model output as the depth at which depth-integrated growth equals depth-integrated losses, or:

$$R(z,t) = \left[\int_{-z}^{0} (\mu_{max} Lim_N Lim_I P) dz\right] - \left[\int_{-z}^{0} \left(gZ + l_{PN}P + l_{PD}P + \frac{\partial}{\partial z}\left(k_D \frac{\partial P}{\partial z}\right)\right) dz + w_P \frac{\partial P}{\partial z}\Big|_{-z}\right] = 0 \quad (9)$$

That is, $H_{cr} = z$, when $R(z,t) = 0$. The values of $R(z,t)$ are plotted in Fig. 11 and show that our estimates of H_{cr} differ significantly from previous analytical calculations: H_{cr} is very deep during the phytoplankton accumulation phase (positive r^*), hence the critical depth criterion ($H_{cr} > H_{MLD}$) holds for all simulations. In our model, the critical depth dramatically deepens in winter (Fig. 11) as a combined result of sufficient nutrient supply, low winter grazing rates and small increases in light. This occurs because our model breaks an initial assumption of the critical depth model: the relationship between phytoplankton growth and loss rates is not constant in time as Sverdrup had assumed (see Sverdrup (1953) assumption 7 and Eq. (6)).

This inadequate assumption affected Sverdrup's critical-depth values and led him to assume the mixed layer shoaling as being key to bloom initiation. Our experimental results about the role of the mixed layer are consistent with considerations in Evans and Parslow (1985): spring blooms develop in the absence of mixed layer fluctuations, and large early blooms are produced when the mixed layer is constantly deep while small delayed ones occur when it is constantly shallow. Nonetheless, the small and delayed blooms simulated with shallow constant mixed layers do not contradict Sverdrup's view of an enhanced phytoplankton

growth due to the mixed layer shoaling. In both, Evans and Parslow's and our experiments, experimental conditions were maintained for several years producing low surface nutrient concentrations and small phytoplankton winter seed populations; hence, they are not testing the effects of shoaling *per se*. The immediate effect of imposing shallow mixed layers under non-limiting nutrient conditions is indeed an abrupt increase in phytoplankton biomass (see experiment II).

The main effects of the mixed layer fluctuations in our experimental results are the modification of nutrient availability in the euphotic zone, and the control of phytoplankton losses below the mixed layer, which is thought to act as a driver for phytoplankton species succession (Margalef, 1978). Deep mixed layers not only supply the amount of nutrients that determines bloom magnitude, but may also allow fast-sinking species, such as diatoms, to return to the euphotic zone (Lande and Wood, 1987) and become part of the seed population that dominates early stages of the spring bloom. On the other hand, the shallowing of the mixed layer plays an important role in nutrient depletion and selection of slow-sinking species, which are characteristic of the fall and winter phytoplankton composition.

An enhancement of phytoplankton growth due to improved light exposure is also observed in the zooplankton dilution experiment (experiment III) where, despite high grazing and low winter nutrient availability, a shallow winter mixed layer produces higher winter phytoplankton biomass and inventory accumulation rates than those obtained using a deep winter mixed layer. Therefore, our results show that the critical-depth criterion is always satisfied when the system achieves positive net phytoplankton accumulation rates and that improvement in light availability due to mixed layer shallowing as envisioned by Sverdrup occurs in our model, however it is not a strictly required process for the spring bloom initiation.

5.2. Is the optimized model consistent with the dilution-recoupling hypothesis?

The simulated zooplankton annual cycles (Figs. 1F and 2) are consistent with top-down control, as proposed by Behrenfeld (2010), in that the deepening of the mixed layer, which in the forcing data begins in August, may contribute to phytoplankton survival during winter by relieving grazing pressure. Moreover, the results of our experiments with zooplankton dilution agree with incubation experiments (e.g., Landry, 1993; Putland, 2000) in the sense that high maximum accumulation rates are achieved when zooplankton biomass is low (Fig. 9B), and when winter dilution is increased (Fig. 9G). Similar to our discussion about the critical-depth hypothesis, in discussing the dilution-recoupling hypothesis we distinguish its two main statements: (1) the spring bloom starts as the consequence of a decoupling between total phytoplankton growth and losses and (2) the main reason for this decoupling is a decrease in zooplankton grazing caused by dilution when the mixed layer deepens.

In Fig. 12, we show that our optimized model meets the first statement. Phytoplankton losses (i.e., grazing + mortality + respiration) vertically integrated over the entire model domain closely match phytoplankton growth throughout the year. Slight imbalances (i.e., a "decoupling") between total growth and losses occur prior to both the spring and fall blooms, the spring bloom being the larger and roughly starting in January. Following Behrenfeld (2010)'s methodology (i.e., r^* and Day^{r*}), the imbalances can occur as early as October of the year preceding the spring bloom. Regardless of whether we integrate the entire vertical water column or use Behrenfeld (2010)'s methodology, the imbalance leading to spring bloom development occurs prior to the shoaling of the mixed layer.

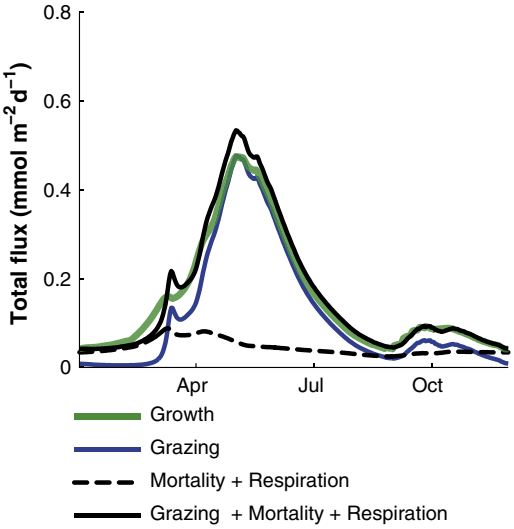

Fig. 12. Phytoplankton growth and loss (grazing, mortality, respiration) rates, vertically integrated over the model domain (total flux in mmol m^{-2} d^{-1}). Small imbalances or "decoupling" between total growth and losses determine the bloom initiation and termination.

Our results do not support the second statement. Under a realistic model configuration, represented by the optimized model, the effects of changes in grazing parameters on initiation of positive accumulation rates (Day^{r*}) are negligible (<6 days); however the grazing parameters affect maximum phytoplankton concentrations. Even when the shoaling of the mixed layer is assumed to actively stimulate zooplankton accumulation (experiment I), the overall effect on phytoplankton is small (the dominant effects are feedbacks via the zooplankton response); such that the depth to which zooplankton is diluted is not as important as whether there are sufficient food resources (e.g., experiment II). Behrenfeld et al. (2013) also already acknowledged the dominance of food availability over the zooplankton response, leading them to restate the dilution-recoupling hypothesis as disturbance-recovery hypothesis. Under this broader concept, the decoupling between phytoplankton growth and losses can be caused by any disturbance of ecological or physical nature. For instance, when experimentally imposing changes in zooplankton concentrations that are independent of changes in food availability, significant shifts in bloom initiation can occur (Fig. 10).

In summary, simulated zooplankton populations do strongly modulate phytoplankton biomass throughout the year, and thus an appropriate low grazing (i.e., "decoupling" of growth and grazing rates) is a required condition for phytoplankton to achieve positive growth during winter. As discussed by Strom (2002), systems where growth and grazing are more tightly coupled throughout the entire year will be more stable and less reactive to perturbations (Pimm, 1984), such as events that change the light or nutrient availability.

5.3. Limitations

As in all modeling studies, the results of our experiments are tied to the model's assumptions and limitations, which we discuss here in order to highlight processes that require further investigation to discern between competing hypotheses for the bloom initiation.

Our model represents a system that is highly sensitive to light, zooplankton and nutrients; where parameters involved in phytoplankton growth have the ability of modifying both the shape and maximum magnitude of the phytoplankton biomass annual

cycle, and parameters involved in zooplankton grazing mainly determine the average annual phytoplankton biomass, by modifying phytoplankton concentrations throughout the year without changing the temporal pattern of the annual cycle. Our model also replicates a decoupling between phytoplankton growth and grazing prior to the bloom initiation. This model behavior is probably caused by the inherent lag between phytoplankton and zooplankton that results from the grazing functional form. The sigmoidal grazing function used here produces a slower slope of increase in grazing when phytoplankton concentrations are low, implying a type of threshold feeding behavior. Threshold feeding is originally based on empirical evidence of mesozooplankton feeding (e.g., Frost, 1975; Gismervik and Andersen, 1997; Wickham, 1995) and has been also show to apply to microherbivory (Lessard and Murrell, 1998). Such threshold may respond to nutritional inadequacy of phytoplankton, zooplankton physiology or changes in feeding strategies. Representing grazing in this form for a natural community may also account for phytoplankton evolutionary strategies to prevent grazing, such as morphological and chemical defenses (Strom, 2002). Different grazing functional forms (Gentleman et al., 2003), as well as higher predation functional forms (i.e., zooplankton mortality) can significantly affect the behavior of simple and more complex ecosystem models (Anderson et al., 2010; Edwards and Yool, 2000; Steele and Henderson, 1992). For instance, Mariani et al. (2013) concluded that an increase in biomass, observed on idealized 0D simulations with adaptive grazing, was driven by changes in predation rather than increases in nutrients or light. Furthermore, other processes not resolved by simple models may also affect the zooplankton phenology independently from phytoplankton biomass, such as horizontal advection, changes in zooplankton composition and zooplankton migration patterns (Aita et al., 2003; Ji et al., 2010). Grazing rates at low prey concentrations and on natural plankton assemblages remain a key uncertainty in our understanding of phytoplankton net growth during winter (Strom et al., 2000); in this sense, models depend on field and laboratory observations to properly define their assumptions about prey–predator relationships.

Another limitation of our approach is the analysis of spatially averaged climatologies. The approach is used to gain understanding about the cyclical conditions that lead to an annually recurring bloom development (Evans and Parslow, 1985). Nonetheless, understanding spatial and intraseasonal variations is necessary to better predict regional interannual variability of phytoplankton biomass. Franks (2014) warns about the possibility of representing misleading plankton dynamics with the analysis of spatially averaged climatological properties, because of the highly non-linear behavior of quantities such as phytoplankton growth and turbulence. The seasonal deepening of the mixed layer plays a key role in our simulations to replenish nutrients in the euphotic zone; but our model environment cannot test the role of other factors that can determine bloom initiation by affecting nutrient availability, such as ocean fronts and eddies (Taylor and Ferrari, 2011b; Mahadevan et al., 2012). Moreover, imposed diffusivities effectively redistribute planktonic organisms in the climatological mixed layer in the model, such that more intense high-frequency mixing events may produce different phytoplankton and zooplankton dynamics.

Also concerning our use of the mixed layer depth forcing, large uncertainty exists on the differentiation between the actively mixed layer (i.e., turbulent layer) and mixed layer diagnosed from density profiles (Brainerd and Gregg, 1995; Franks, 2014). For instance, the appearance of spring blooms in unstratified water columns has been explained by weak turbulence (Colebrook, 1979; Townsend et al., 1992; Wasmund et al., 1998; Chiswell, 2011; Huisman et al., 1999a,b) or by the cessation of convective mixing (Fennel, 1999; Taylor and Ferrari, 2011a). In order to fulfill the critical-depth model assumption of a thoroughly mixed top layer, we assumed in our model that the mixing and mixed layer depths are identical. The imposed mixed/mixing depth thus defines a simplified vertical structure for turbulence, which is in reality a highly variable property (Franks, 2014). The vertical structure of turbulence may play a key role in determining the residence time of phytoplankton cells within the euphotic zone (Backhaus et al., 2003; Huisman et al., 2002; Lande and Wood, 1987; Ward and Waniek, 2007). We can argue that the optimized parameters in our model represent a type of phytoplankton community that benefits from intermediate to deep mixing, such that sinking cells are able to recirculate within the euphotic zone. When the constant H_{MLD} is shallow, a large amount of sinking phytoplankton is lost below the mixed layer, resulting in a delayed bloom of lower magnitude. In a more realistic scenario, species succession may determine the dominance of small, slow sinking cells during summer months (Margalef, 1978). Further investigation, combining observations and models, is required to discern whether simplified climatological forcing is indeed representative of the processes leading to the spring bloom development in nature. In particular, it is important to define how the planktonic community as a whole, as well as individual functional groups, react to high-frequency fluctuations in turbulence and the turbulence vertical structure.

Given these limitations, our results support the general idea that under sufficient nutrient supply, improved light conditions in combination with low zooplankton populations allow "turbulence-adapted" cells to initiate the spring bloom.

6. Conclusion

Our optimized and experimental results suggest that the spring bloom initiation cannot be seen as a purely bottom-up or top-down process. The conceptual bases of both, the critical-depth and the dilution-recoupling, hypotheses are shown to be true within our modeling framework and cannot be considered in absolute isolation under realistic simulations. It has to be pointed out that the fundamental ideas of both hypotheses are ecological truisms: (a) positive net growth of phytoplankton occurs when the critical depth is greater than the mixed layer depth (Sverdrup, 1953) and (b) low zooplankton concentrations during winter allow phytoplankton growth to exceed its losses (Behrenfeld, 2010). Under realistic and idealized configurations, both conditions occur in our model prior to a bloom development; however, neither the critical-depth nor the dilution-recoupling hypothesis fully applies during bloom initiation in our experiments.

The bottom-up and top-down approaches mainly diverge on their view of the role that the mixed layer plays in regulating plankton populations. The critical depth model postulates that the shoaling of the mixed layer at the beginning of spring triggers the bloom by enhancing available light for phytoplankton. More specifically, the model predicts that the bloom starts when the mixed layer depth becomes shallower than the critical depth. This implies that the critical depth is shallower than the mixed layer depth in winter – a condition that is not met in our model simulations and also likely not met in reality. Sverdrup's conclusions about the critical depth and the role of stratification onset were probably affected by his assumption of a constant ratio between phytoplankton growth and losses. As noted already by Smetacek and Passow (1990) and Behrenfeld (2010), this assumption is incorrect and also is not met in our model, where a profound critical depth is present during winter, when positive phytoplankton accumulation rates occur. However, maximum phytoplankton accumulation rates and bloom onset do indeed coincide with the time when the mixed layer becomes shallower than the critical depth.

An imbalance or "decoupling" of growth and grazing rates occurs prior to bloom development, but it occurs as result of ecological feedbacks rather than physical forcings as had been postulated in the dilution-recoupling hypothesis. Nonetheless, appropriate low grazing should be seen as a required condition for bloom development to the same extend that phytoplankton light and nutrient requirements have to be satisfied. In this sense, there might not exist a unique "trigger" for the spring bloom initiation but it will depend on the system's base line conditions at the end of the preceding year, and the bloom development may closely track the last of these "bloom-forming conditions" that remains unsatisfied. Overall, caution should be used when extrapolating experimental conclusions to reality.

Acknowledgements

We thank M. Behrenfeld for providing the chlorophyll and mixed layer depth climatological annual cycles, as well as insightful comments on the manuscript. We also gratefully acknowledge NSERC Discovery and MEOPAR funding.

Appendix A. Supplementary material

Supplementary data associated with this article can be found, in the online version, at http://dx.doi.org/10.1016/j.pocean.2015.07.004.

References

Aita, M.N., Yamanaka, Y., Kishi, M., 2003. Effects of ontogenetic vertical migration of zooplankton on annual primary production – using NEMURO embedded in a general circulation model. Fisheries Oceanography 12, 284–290.

Anderson, T.R., 2005. Plankton functional type modelling: running before we can walk? Journal of Plankton Research 27, 1073–1081.

Anderson, T.R., Gentleman, W.C., Sinha, B., 2010. Influence of grazing formulations on the emergent properties of a complex ecosystem model in a global ocean general circulation model. Progress in Oceanography 87, 201–213.

Backhaus, J.O., Hegseth, E.N., Wehde, H., Irigoien, X., Hattern, K., Logemann, K., 2003. Convection and primary production in winter. Marine Ecology Progress Series 251, 1–14.

Bagniewski, W., Fennel, K., Perry, M.J., D'Asaro, E., 2011. Optimizing models of the North Atlantic spring bloom using physical, chemical and bio-optical observations from a Lagrangian float. Biogeosciences 8, 1291–1307. http://dx.doi.org/10.5194/bg-8-1291-2011.

Banse, K., 1994. Grazing and zooplankton production as key controls of phytoplankton production in the open ocean. Oceanography 7, 13–20.

Behrenfeld, M.J., 2010. Abandoning Sverdrup's critical depth hypothesis on phytoplankton blooms. Ecology 91, 977–989.

Behrenfeld, M.J., Boss, E., 2006. Beam attenuation and chlorophyll concentration as alternative optical indices of phytoplankton biomass. Journal of Marine Research 64, 431–451.

Behrenfeld, M.J., Boss, E., 2003. The beam attenuation to chlorophyll ratio: an optical index of phytoplankton physiology in the surface ocean? Deep Sea Research I 50, 1537–1549.

Behrenfeld, M.J., Boss, E., Siegel, D.A., Shea, D.M., 2005. Carbon-based ocean productivity and phytoplankton physiology from space. Global Biogeochemical Cycles 19.

Behrenfeld, M.J., Doney, S.C., Lima, I., Boss, E., Siegel, D.A., 2013. Annual cycles of ecological disturbance and recovery underlying the subartic Atlantic spring plankton bloom. Global Biogeochemical Cycles 27, 526–540. http://dx.doi.org/10.1002/gbc.20050.

Bienfang, P.K., 1981. Sinking rates of heterogeneous, temperate phytoplankton populations. Journal of Plankton Research 3, 235–253.

Bopp, L., Aumont, O., Cadule, P., Alvain, S., Gehlen, M., 2005. Response of diatoms distribution to global warming and potential implications: a global model study. Geophysical Research Letters 32, 1–4.

Boss, E., Behrenfeld, M.J., 2010. In situ evaluation of the initiation of the North Atlantic phytoplankton bloom. Geophysical Research Letters 37.

Brainerd, K.E., Gregg, M.C., 1995. Surface mixed and mixing layer depths. Deep-Sea Research I 42, 1521–1543.

Brock, T.D., 1981. Calculating solar radiation for ecological studies. Ecological Modelling 14, 1–19.

Brody, S.R., Lozier, M.S., Dunne, J.P., 2013. A comparison of methods to determine phytoplankton bloom initiation. Journal of Geophysical Research: Oceans 118, 1–13.

Chiswell, S.M., 2011. Annual cycles and spring blooms in phytoplankton: don't abandon Sverdrup completely. Marine Ecology Progress Series 443, 39–50. http://dx.doi.org/10.3354/meps09453.

Colebrook, J.M., 1979. Continuous plankton records: seasonal cycles of phytoplankton and copepods in the North Atlantic Ocean and the North Sea. Marine Biology 51, 23–32.

Colman, R.A., Power, S.B., McAvaney, B.J., 1997. Non-linear climate feedback analysis in an atmospheric general circulation model. Climate Dynamics 13, 717–731.

Dall'Olmo, G., Westberry, T.K., Behrenfeld, M.J., Boss, E., Slade, W.H., 2009. Significant contribution of large particles to optical backscattering in the open ocean. Biogeosciences 6, 947–967.

de Boyer Montégut, C., Madec, G., Fischer, A.S., Lazar, A., Iudicone, D., 2004. Mixed layer depth over the global ocean: An examination of profile data and a profile-based climatology. Journal of Geophysical Research 109, 1–20. http://dx.doi.org/10.1029/2004JC002378.

Denman, K.L., 2003. Modelling planktonic ecosystems: parameterizing complexity. Progress in Oceanography 57, 429–452.

Doney, S., Glover, D., Najjar, R., 1996. A new coupled, one-dimensional biological-physical model for the upper ocean: applications to the JGOFS Bermuda Atlantic Time series Study (BATS) site. Deep-Sea Research II 4, 591–624.

Edwards, A.M., Yool, A., 2000. The role of higher predation in plankton population models. Journal of Plankton Research 22, 1085–1112.

Eppley, R.W., 1972. Temperature and phytoplankton growth in the sea. Fishery Bulletin 70, 1063–1085.

Evans, G., Parslow, J.S., 1985. A model of annual plankton cycles. Biological Oceanography 3, 327–347.

Fahnenstiel, G.L., McCormick, M.J., Lang, G.A., Redalje, D.G., Lohrenz, S.E., Markowitz, M., Wagoner, B., Carrick, H., 1995. Taxon-specific growth and loss rates for dominant phytoplankton populations from the northern Gulf of Mexico. Marine Ecology Progress Series 117, 229–239.

Fasham, M.J.R., Ducklow, H.W., McKelvie, S.M., 1990. A nitrogen based model of plankton dynamics in the oceanic mixed layer. Journal of Marine Research 48, 591–639.

Fennel, K., 1999. Convection and the timing of phytoplankton spring blooms in the Western Baltic Sea. Estuarine, Coastal and Shelf Science 49, 113–128.

Fennel, K., Losch, M., Schröter, J., Wenzel, M., 2001. Testing a marine ecosystem model: sensitivity analysis and parameter optimization. Journal of Marine Systems 28, 45–63.

Fennel, K., Wilkin, J., Levin, J., Moisan, J., O'Reilly, J.E., Haidvogel, D., 2006. Nitrogen cycling in the Middle Atlantic Bight: results from a three-dimensional model and implications for the North Atlantic nitrogen budget. Global Biogeochemical Cycles 20, 14. http://dx.doi.org/10.1029/2005GB002456.

Franks, P.J., 2014. Has Sverdrup's critical depth hypothesis been tested? Mixed layers vs. turbulent layers. ICES Journal of Marine Science. http://dx.doi.org/10.1093/icesjms/fsu175.

Franks, P.J., Di Lorenzo, E., Goebel, N.L., Chenillat, F., Riviere, P., Edwards, C.A., Miller, A.J., 2013. Modelling physical-biological responses to climate change in the California Current System. Oceanography 3, 26–33.

Franks, P.J., Wroblewski, J.S., Flierl, G.R., 1986. Behavior of a simple plankton model with food-level acclimation by herbivores. Marine Biology 91, 121–129.

Friedrichs, M.A.M., Dusenberry, J.A., Anderson, L.A., Armstrong, R.A., Chai, F., Christian, J.R., Doney, S., Dunne, J.P., Fujii, M., Hood, R., McGillicuddy, D.J., Moore, K., Schartau, M., Spitz, Y.H., Wiggert, J., 2007. Assessment of skill and portability in regional marine biogeochemical models: role of multiple planktonic groups. Journal of Geophysical Research 112, 1–22.

Frost, B.W., 1975. A threshold feeding behavior in Calanus pacificus. Limnology and Oceanography 20, 263–266.

Garcia, H.E., Locarnini, R.A., Boyer, T.P., Antonov, J.I., Zweng, M.M., Baranova, O.K., Johnson, D.R., 2010. Nutrients (phosphate, nitrate, and silicate). In: World Ocean Atlas 2009, NOAA Atlas NESDIS 71. U.S. Government Printing Office, Washington, DC, p. 398.

Garside, C., Garside, J.C., 1993. The "f-ratio" on 20°W during the North Atlantic Bloom Experiment. Deep Sea Research Part II: Topical Studies in Oceanography 40, 75–90.

Garver, S.A., Siegel, D.A., 1997. Inherent optical property inversion of ocean color spectra and its biogeochemical interpretation: 1. Time series from the Sargasso Sea. Journal of Geophysical Research 102, 18607–18625.

Geider, R.J., 1987. Light and temperature dependence of the carbon to chlorophyll a ratio in microalgae and cyanobacteria: implications for physiology and growth of phytoplankton. New Phytologist 106, 1–34.

Geider, R.J., MacIntyre, H.L., Kana, T.M., 1997. Dynamic model of phytoplankton growth and acclimation: responses of the balanced growth rate and the chlorophyll a: carbon ratio to light, nutrient-limitation and temperature. Marine Ecology Progress Series 148, 187–200.

Gentleman, W., Leising, A., Frost, B., Strom, S., Murray, J., 2003. Functional responses for zooplankton feeding on multiple resources: a review of assumptions and biological dynamics. Deep-Sea Research II 50, 2847–2875.

Gifford, D., Fessenden, L., Garrahan, P.R., Martin, E., 1995. Grazing by microzooplankton and mesozooplankton in the high-latitude North Atlantic Ocean: Spring versus summer dynamics. Journal of Geophysical Research 10, 6665–6675. http://dx.doi.org/10.1029/94JCC00983.

Gismervik, I., Andersen, T., 1997. Prey switching by *Acartia clausi* experimental evidence and implications of intraguil predation assessed by a model. Marine Ecology Progress Series 157, 247–259.

Henson, S.A., Dunne, J.P., Sarmiento, J.L., 2009. Decadal variability in North Atlantic phytoplankton blooms. Journal of Geophysical Research 114, 1–11.
Henson, S.A., Robinson, I., Allen, J.T., Waniek, J.J., 2006. Effect of meteorological conditions on interannual variability in timing and magnitude of the spring bloom in the Irminger Basin, North Atlantic. Deep-Sea Research I 53, 1601–1615.
Houck, C.R., Joines, J.A., Kay, M.G., 1995. A Genetic Algorithm for Function Optimization: A Matlab Implementation (Technical Report No. NCSU-IE-TR-95-09). North Carolina State University, Raleigh, NC.
Huisman, J., Arrayas, M., Ebert, U., Sommeijer, B., 2002. How do sinking phytoplankton species manage to persist? The American Naturalist 159, 245–254.
Huisman, J., van Oostveen, P., Weissing, F.J., 1999a. Species dynamics in phytoplankton blooms: incomplete mixing and competition for light. The American Naturalist 154, 46–68.
Huisman, J., van Oostveen, P., Weissing, F.J., 1999b. Critical depth and critical turbulence. Two different mechanisms for the development of phytoplankton blooms. Limnology and Oceanography 44, 1781–1787.
Ji, R., Edwards, M., Mackas, D.L., Runge, J., Thomas, A., 2010. Marine plankton phenology and life history in a changing climate: current research and future directions. Journal of Plankton Research 32, 1355–1368.
Joos, F., Plattner, G.-K., Stocker, T., Marchal, O., Schmittner, A., 1999. Global warming and marine carbon cycle feedbacks on future atmospheric CO_2. Science 284, 464–467.
Lande, R., Wood, M., 1987. Suspension times of particles in the upper ocean. Deep Sea Research Part A. Oceanographic Research Papers 1, 61–72.
Landry, M.R., 1993. Estimating rates of growth and grazing mortality of phytoplankton by the dilution method. In: Handbook of Methods in Aquatic Microbial Ecology. Lewis Publishers, Boca Raton, pp. 715–721.
Landry, M.R., Hassett, R.P., 1982. Estimating the grazing impact of marine micro-zooplankton. Marine Biology 67, 283–288.
Landry, M.R., Hasset, R.P., Fagerness, V., Downs, J., Lorenzen, C.J., 1984. Effect of food acclimation on assimilation efficiency of *Calanus pacificus*. Limnology and Oceanography 29, 361–364.
Lessard, E.J., Murrell, M.C., 1998. Microzooplankton herbivory and phytoplankton growth in the northwestern Sargasso Sea. Aquatic Microbial Ecology 16, 173–188.
Lewis, K., Allen, J.I., Richardson, A.J., Holt, J.T., 2006. Error quantification of a high resolution coupled hydrodynamic ecosystem coastal-ocean model: Part3, validation with Continuous Plankton Recorder data. Journal of Marine Systems 63, 209–224.
Mahadevan, A., D'Asaro, E., Lee, C., Perry, M.J., 2012. Eddy-driven stratification initiates North Atlantic spring phytoplankton blooms. Science 337. http://dx.doi.org/10.1126/science.1218740.
Maier-Reimer, E., Mikolajewicz, U., Winguth, A., 1996. Future ocean uptake of CO_2: interaction between ocean circulation and biology. Climate Dynamics 12, 711–721.
Margalef, R., 1978. Life-forms of phytoplankton as survival alternatives in an unstable environment. Oceanologica Acta 1, 493–509.
Mariani, P., Andersen, K.H., Visser, A.W., Barton, A.D., Kiørboe, T., 2013. Control of plankton seasonal succession by adaptive grazing. Limnology and Oceanography 58, 173–184.
Maritorena, S., Siegel, D.A., Peterson, A.R., 2002. Optimization of a semianalytical ocean color model for global-scale applications. Applied Optics 41, 2705–2714.
Miller, C.B., Frost, B.W., Booth, B., Wheeler, P., Landry, M.R., Welschmeyer, N.A., 1991. Ecological processes in the Subartic Pacific: iron limitation cannot be the whole story. Oceanography 4, 71–78.
Nejstgaard, J.C., Gismervikz, I., Solberg, P.T., 1997. Feeding and reproduction by *Calanus finmarchicus*, and microzooplantkon grazing during mesocosm blooms of diatoms and the coccolithophore *Emiliania huxleyi*. Marine Ecology Progress Series 147, 197–217.
Nejstgaard, J.C., Hygum, B.H., Naustvoll, L.J., Båmstedt, U., 2001. Zooplankton growth, diet and reproductive success compared in simultaneous diatom- and flagellate- microzooplankton-dominated plankton blooms. Marine Ecology Progress Series 221, 77–91.
Pimm, S.L., 1984. The complexity and stability of ecosystems. Nature 307, 321–326.
Platt, T., Bird, D.F., Sathyendranath, S., 1991. Critical depth and marine primary production. Proceedings of the Royal Society of London, Series B: Biological Sciences 246, 205–217.
Platt, T., White III, G.N., Zhai, L., Sathyendranath, S., Roy, S., 2009. The phenology of phytoplankton blooms: ecosystem indicators from remote sensing. Ecological Modelling 220, 3057–3069. http://dx.doi.org/10.106/J.ECOLMODEL.2008.11.022.
Previdi, M., Fennel, K., Wilkin, J., Haidvogel, D., 2009. Interannual variability in atmospheric CO_2 uptake on the northeast U.S. continental shelf. Journal of Geophysical Research 114, 13.
Putland, J.N., 2000. Microzooplankton herbivory and bacterivory in Newfoundland coastal waters during spring, summer and winter. Journal of Plankton Research 22, 253–277.
Riley, G.A., 1965. A mathematical model. Limnology and Oceanography 10, 202–215.
Sarmiento, J.L., Hughes, T.M.C., Stouffer, R.J., Manabe, S., 1998. Simulated response of the ocean carbon cycle to anthropogenic climate warming. Nature 393.
Sarthou, G., Timmermans, K.R., Blain, S., Tréguer, P., 2005. Growth physiology and fate of diatoms in the ocean: a review. Journal of Sea Research 53, 25–42.
Schartau, M., Oschlies, A., 2003. Simultaneous data-based optimization of a 1D-ecosystem model at three locations in the North Atlantic: Part I – method and parameter estimates. Journal of Marine Research 61, 765–793.
Schartau, M., Oschlies, A., Jürgen, W., 2001. Parameter estimates of a zero-dimensional ecosystem model applying the adjoint method. Deep-Sea Research II 48, 1769–1800.
Siegel, D.A., Doney, S.C., Yoder, J.A., 2002. The North Atlantic spring phytoplankton bloom and Sverdrup's critical depth hypothesis. Science 296, 730–733 (Reports).
Siegel, D.A., Maritorena, S., Nelson, N.B., Behrenfeld, M.J., 2005. Independence and interdependencies among global ocean color properties: reassessing the bio-optical assumption. Journal of Geophysical Research 110. http://dx.doi.org/10.1029/2004JC002527.
Smayda, T., 1974. Some experiments on the sinking characteristics of two freshwater diatoms. Limnology and Oceanography 19, 628–635.
Smayda, T., Bienfang, P.K., 1983. Suspension properties of various phyletic groups of phytoplankton and tintinnids in an oligotrophic, subtropical system. Marine Ecology 4, 289–300.
Smetacek, V., Passow, U., 1990. Spring bloom initiation and Sverdrup's critical depth model. Limnology and Oceanography 35, 228–234.
Smith, E.L., 1936. Photosynthesis in relation to light and carbon dioxide. Proceedings of the National Academy of Sciences of the United States of America 22, 504–511.
Steele, J.H., Henderson, E.W., 1992. The role of predation in plankton models. Journal of Plankton Research 14, 157–172.
Strom, S., 2002. Novel interactions between phytoplankton and microzooplankton: their influence on the coupling between growth and grazing rates in the sea. Hydrobiologia 480, 41–54.
Strom, S., Miller, C.B., Frost, B.W., 2000. What sets lower limits to phytoplankton stocks in high-nitrate, low-chlorophyll regions of the open ocean? Marine Ecology Progress Series 193, 19–31.
Sverdrup, H.U., 1953. On conditions for vernal blooming of phytoplankton. Journal du Conseil 18, 287–295.
Tande, K.S., Slagstad, D., 1985. Assimilation efficiency in herbivorous aquatic organisms - The potential of the ratio method using ^{14}C and biogenic silica as markers. Limnology and Oceanography 30, 1093–1099.
Taylor, J.R., Ferrari, R., 2011a. Shutdown of turbulent convection as a new criterion for the onset of spring phytoplankton blooms. Limnology and Oceanography 56, 2293–2307.
Taylor, J.R., Ferrari, R., 2011b. Ocean fronts trigger high latitude phytoplankton blooms. Geophysical Research Letters 38, 5. http://dx.doi.org/10.1029/2011GL049312.
Townsend, D.W., Keller, M.D., Sieracki, M.E., Ackleson, S.G., 1992. Spring phytoplankton blooms in the absence of vertical water column stratification. Nature 360, 59–62.
Veldhuis, M.J., Timmermans, K.R., Croot, P., van der Wagt, B., 2005. Picophytoplankton: a compartive study of their biochemical composition and photosynthetic properties. Journal of Sea Research 53, 7–24. http://dx.doi.org/10.1016/j.seares.2004.01.006.
Wang, X.J., Behrenfeld, M.J., Le Borge, R., Murtugudde, R., Boss, E., 2009. Regulation of phytoplankton carbon to chlorophyll ratio by light, nutrients and temperature in the Equatorial Pacific Ocean: a basin-scale model. Biogeosciences 6, 391–404.
Walsby, A.E., Holland, D.P., 2006. Sinking velocities of phytoplankton measured on a stable density gradient by laser scanning. Journal of the Royal Society Interface 3, 429–439.
Ward, B.A., Friedrichs, M.A.M., Anderson, T.R., Oschlies, A., 2010. Parameter optimization techniques and the problem of underdetermination in marine biogeochemical models. Journal of Marine Systems 81, 34–43.
Ward, B.A., Waniek, J.J., 2007. Phytoplankton growth conditions during autumn and winter in the Irminger Sea, North Atlantic. Marine Ecology Progress Series 334, 47–61.
Wasmund, N., Nausch, G., Matthaus, W., 1998. Phytoplankton spring blooms in the southern Baltic Sea: spatio-temporal development and long-term trends. Journal of Plankton Research 20, 1099–1117.
Westberry, T.K., Behrenfeld, M.J., Siegel, D.A., Boss, E., 2008. Carbon-based primary productivity modeling with vertical resolved photoacclimation. Global Biogeochemical Cycles 22.
Wickham, S.A., 1995. Cyclops predation on ciliates: species-species differences and functional responses. Journal of Plankton Research 17, 1633–1646.